NASA TECHNICAL NOTE

NASA TN D-6827

NASA TN D-6827

FLIGHT CALIBRATION OF COMPENSATED AND UNCOMPENSATED PITOT-STATIC AIRSPEED PROBES AND APPLICATION OF THE PROBES TO SUPERSONIC CRUISE VEHICLES

by Lannie D. Webb and Harold P. Washington

Flight Research Center
Edwards, Calif. 93523

NATIONAL AERONAUTICS AND SPACE ADMINISTRATION • WASHINGTON, D. C. • MAY 1972

1. Report No.	2. Government Accession No.	3. Recipient's Catalog No.
NASA TN D-6827		

4. Title and Subtitle	5. Report Date
FLIGHT CALIBRATION OF COMPENSATED AND UNCOMPENSATED PITOT-STATIC AIRSPEED PROBES AND APPLICATION OF THE PROBES TO SUPERSONIC CRUISE VEHICLES	May 1972
	6. Performing Organization Code

7. Author(s)	8. Performing Organization Report No.
Lannie D. Webb and Harold P. Washington	H-665
	10. Work Unit No.
9. Performing Organization Name and Address	761-74-02-00-24
NASA Flight Research Center P. O. Box 273 Edwards, California 93523	11. Contract or Grant No.
	13. Type of Report and Period Covered
12. Sponsoring Agency Name and Address	Technical Note
National Aeronautics and Space Administration Washington, D. C. 20546	14. Sponsoring Agency Code

15. Supplementary Notes

16. Abstract

Static-pressure position-error calibrations for a compensated and an uncompensated XB-70 nose-boom pitot-static probe were obtained in flight. The methods (Pacer, acceleration-deceleration, and total temperature) used to obtain the position errors over a Mach number range from 0.5 to 3.0 and an altitude range from 7600 meters (25,000 feet) to 21,000 meters (70,000 feet) are discussed. The error calibrations are compared with the position error determined from wind-tunnel tests, theoretical analysis, and a standard NACA pitot-static probe. Factors which influence position errors, such as angle of attack, Reynolds number, probe tip geometry, static-orifice location, and probe shape, are discussed. Also included are examples showing how the uncertainties caused by position errors can affect the inlet controls and vertical altitude separation of a supersonic transport.

17. Key Words (Suggested by Author(s))	18. Distribution Statement
Pitot-static probes	Unclassified - Unlimited

19. Security Classif. (of this report)	20. Security Classif. (of this page)	21. No. of Pages	22. Price*
Unclassified	Unclassified	40	$3.00

*For sale by the National Technical Information Service, Springfield, Virginia 22151

CONTENTS

FLIGHT CALIBRATION OF COMPENSATED AND UNCOMPENSATED PITOT-STATIC AIRSPEED PROBES AND APPLICATION OF THE PROBES TO SUPERSONIC CRUISE VEHICLES

Lannie D. Webb and Harold P. Washington
Flight Research Center

INTRODUCTION

Precise knowledge of Mach number and altitude is of utmost importance for supersonic cruise aircraft. The information is necessary for both pilot displays and automatic systems. Even greater precision is required for evaluating the aircraft and the propulsion system performance in flight. Seemingly minor errors in the measurement of free-stream static pressure greatly affect the measurement of inlet recovery and the range of the aircraft.

It has been common practice to calibrate nose-boom pitot-static systems in wind-tunnel tests and in flight only through the transonic speed region and either to assume that there was no supersonic error or to extrapolate the usually small supersonic error to higher speeds. Experience with the XB-70 airplane (fig. 1) showed that neither practice is adequate. In some instances wind-tunnel calibrations of pitot-static probes at high supersonic speeds may also be inadequate unless the wind-tunnel tests provide for very accurate measurements under simulated flight conditions.

The XB-70 airplane was flight-tested initially with a compensated pitot-static probe which had a specially contoured shape near the static-pressure ports (ref. 1). This probe was designed to reduce the measured position error experienced by uncompensated pitot-static probes at transonic speeds and to maintain a minimal position error at supersonic speeds. Early XB-70 flight tests produced inconsistent supersonic calibration data. Because the reasons for the nonrepeatability of the data could not be determined from the flight data, wind-tunnel tests were conducted at the NASA Langley Research Center by Virgil S. Ritchie and Frank L. Jordan, Jr. Subsequently, the compensated pitot-static probe was replaced by a more conventional uncompensated pitot-static probe (modified MA-I type). Although the uncompensated probe produced a larger subsonic position error than the compensated probe, the supersonic data were more consistent.

In this report flight and wind-tunnel data are combined to form a complete position-error calibration. Position-error data from flight and wind-tunnel tests for both compensated and uncompensated pitot-static probes are analyzed and compared with data from other types of pitot-static probes. The effects of Reynolds number and angle of attack on the data obtained from the pitot-static probes used on the XB-70 airplane are discussed. The implications of using these types of probes on supersonic transports or other aircraft operating at high speeds and altitudes are also discussed.

SYMBOLS

Physical quantities in this report are given in the International System of Units (SI) and parenthetically in U.S. Customary Units. Measurements were taken in Customary Units. Factors relating the two systems are presented in reference 2.

h_r	geometric (radar) altitude, meters (feet)
$h_{p,\infty}$	true pressure altitude, meters (feet)
Δh	true pressure altitude minus indicated pressure altitude, meters (feet)
$p_{t,2}$	stagnation pressure, newtons/meter^2 (pounds/inch^2)
p_∞	ambient pressure, newtons/meter^2 (pounds/inch^2)
Δp	indicated static pressure minus ambient pressure, newtons/meter^2 (pounds/inch^2)
M_i	indicated Mach number
M_∞	true Mach number
ΔM	true Mach number minus indicated Mach number
R	Reynolds number, per meter (foot)
S_1/S_2	rearward manifolded static orifices (for both compensated and uncompensated pitot-static probes)
S_3	forward manifolded static orifices (for both compensated and uncompensated pitot-static probes)
T_o	total temperature, degrees Kelvin or degrees Celsius (degrees Rankine or degrees Fahrenheit)
T_∞	ambient temperature, degrees Kelvin or degrees Celsius (degrees Rankine or degrees Fahrenheit)
ΔT_o	uncertainty in the measurement of total temperature
ΔT_∞	uncertainty in the measurement of ambient temperature
α	angle of attack, degrees
γ	specific-heat ratio, 1.4

$\Delta\gamma$ uncertainty in the measurement of specific-heat ratio

ϵ recovery factor

DESCRIPTION OF APPARATUS

Onboard Sensors

Photos of the compensated and uncompensated pitot-static probes used on the XB-70 aircraft are shown in figure 2. Dimensions of the probes and the nose-boom assembly are shown in figures 3 and 4, respectively.

As shown in figure 4, the nose boom was inclined downward at an angle of 4.17° (referenced to the aircraft's centerline) for approximate alinement of the pitot-static probe with the relative wind during cruise flight conditions. Both types of probes used on the XB-70 airplane were equipped with dual sets of static orifices which were separated by 2.54 centimeters (1 inch) (fig. 3). The S_3 orifices were connected to the XB-70 plenum chamber reference tank system and the cockpit instruments. The primary source of airspeed data was the rear set of static orifices (S_1/S_2), which was connected to the recording pressure transducers and the central air data computer. Both the compensated and the uncompensated pitot-static probes were mounted so that the S_1/S_2 orifices were 180.8 centimeters (71.2 inches) from the apex of the nose of the airplane, as illustrated in figure 4. Both installations incorporated angle-of-attack and angle-of-sideslip vanes.

Two total-temperature probes were mounted on the XB-70 airplane below and 152.4 centimeters (60 inches) back of the apex edge of the inlet ramp, as illustrated in figure 5(a). The dimensions of the probes and a photograph are shown in figures 5(b) and 5(c), respectively. Each probe consisted of two platinum, open-wire, resistance windings enclosed in three radiation shields. One total-temperature probe measured temperatures from -68° C (-90° F) to 171° C (340° F) and the other from 133° C (272° F) to 396° C (745° F). One platinum element in each probe provided data for the central air data computer, and the other element provided data to a magnetic recording tape within the instrumentation package.

Onboard Recording Instrumentation

The total and static pressures from the pitot-static probes were measured by specially built unbonded strain gage pressure transducers, which were coupled directly to a 13-bit digital encoder. The output of these transducers, together with that of the air data computer and the total-temperature probes, was recorded by the airborne data acquisition system (ref. 3).

To use the special pressure transducers, a 2-hour warmup was required before takeoff. Preflight and postflight zeros were obtained just before takeoff and just after landing and were compared to an aneroid barometer reading.

Radar and Meteorological Apparatus

Ground radars such as FPS-16, MPS-25, and SCR-584 units were used to track the XB-70 airplane to obtain its true geometric altitude. The ambient pressure and temperature at the radar-measured geometric altitude were obtained from an AN/AMT-4B rawinsonde balloon (ref. 4) released by the Air Force Air Weather Service, Edwards Air Force Base, Calif., at XB-70 takeoff. Atmospheric data from the radiosonde package were transmitted to an AN/GMD-1A rawin set (ref. 5) and recorded on magnetic tape for subsequent data reduction (ref. 6).

FLIGHT CALIBRATION PROCEDURES AND WIND-TUNNEL TESTS

Because of the large speed and altitude capability of the XB-70 airplane, several conventional and unconventional calibration procedures were used to obtain an airspeed calibration of the pitot-static probes. As illustrated in figure 6, conventional stabilized Pacer data were obtained in the subsonic speed region, whereas an unconventional radar tracking acceleration and deceleration technique was the primary source of airspeed data in the transonic and supersonic speed regions. The total-temperature probe was also used in the supersonic region. Wind-tunnel data helped to establish the final position-error curve at the higher supersonic Mach numbers.

Pacer Method

Two U.S. Air Force calibrated Pacer (ref. 7) aircraft, a T-38 and an F-104, were used to calibrate the XB-70 position error in the subsonic Mach number range. During the airspeed calibration runs, the XB-70 airplane was stabilized at a predetermined altitude and Mach number. Next, the calibrated Pacer was stabilized alongside the XB-70 airplane. Indicated airspeed and pressure altitude were recorded by the cockpit camera in the Pacer aircraft. After these quantities were corrected for instrument and position error, they were correlated with the measured XB-70 pitot and static pressures to determine the static-pressure position error.

Acceleration-Deceleration Radar Method

An unconventional method--the acceleration-deceleration radar method--was used to calibrate the static-pressure position error of the pitot-static airspeed installation on the XB-70 airplane at high altitudes and at transonic and supersonic speeds. A precision radar-transponder system determined the geometric height of the airplane as it accelerated or decelerated at various pressure altitudes. During these test runs, measurements were made continuously with the pitot-static installation. True ambient pressure at a given geometric height was determined by flying the airplane at a speed for which the static-pressure error had been determined previously by an accepted method of obtaining an airspeed calibration, such as a tower flyby, a Pacer aircraft, radar plus rawinsonde balloon, a trailing cone, or a smoke trail laid by a Pacer aircraft.

Because true ambient pressure, and, hence, true pressure altitude, was known at

a referenced Mach number, any small change in geometric height was assumed to correspond to a like change in pressure altitude during the calibration runs. Thus, for the Mach number range traversed during the XB-70 tests, the true pressure altitude was known and could be converted readily to true ambient pressure by using standard atmospheric tables or equations.

With this method, if the entire Mach number range of the test airplane could not be traversed at one test altitude, an overlapping acceleration-deceleration technique was used. The technique consisted of flying another acceleration or deceleration maneuver at a different altitude at which a larger Mach number range could be covered. The two sets of data were combined if the second acceleration or deceleration maneuver included part of the same Mach number range as the first. The maximum Mach number reached on the second acceleration or deceleration run was used as a second "reference" Mach number. This second Mach number was then used as the reference condition at higher altitudes, and the process was repeated until the entire Mach number range was covered.

The XB-70 tests were started at a Mach number of 0.90 and an altitude of 9750 meters (32,000 feet). At this altitude, the airplane could easily accelerate from this subsonic Mach number, at which the static-pressure error was known, through the transonic Mach region, to a "limit" Mach number near 1.4. Because this limit speed was less than the maximum speed capability of the airplane (fig. 6), additional calibration runs were performed at higher altitudes where the airplane could operate at higher Mach numbers (fig. 7).

The static-pressure error determined near a Mach number of 1.4 was used as the reference point for the higher altitude at which the tests were performed. For the XB-70 airplane, this would have required acceleration from a Mach number of approximately 1.4 to the limit speed at the higher altitude. This procedure was not operationally feasible, however, because of the reduced acceleration potential of the XB-70 airplane at the higher altitudes. Decelerations were found to be more practical because the entire maneuver could be conducted within the test range of the radars and did not consume excessive quantities of fuel and test time. The results were essentially the same as for accelerations.

The primary advantages of this method were (1) minimization of dependence on transmitted radiosonde measurements, (2) simplicity of flight scheduling, (3) ease of testing, (4) minimization of the lag problem at high altitudes, and (5) speed and accuracy in obtaining an airspeed calibration for the entire Mach range of the test aircraft. Care was taken to match angles of attack and Reynolds numbers when different acceleration and deceleration runs were performed.

Total-Temperature Method

Static-pressure position error was determined also by a total-temperature method in which indicated static pressure, total temperature, and ambient temperature were used. The XB-70 flight data selected for analysis were for level flight when the aircraft was closer than approximately 110 kilometers (70 miles) to the rawinsonde balloon. Data obtained from the high- and low-range total-temperature probes in the overlapping temperature range (approximately 149° C (300° F)) were compared to

check the performance of the probes.

Mach number was obtained from the total-temperature measurements by using the ideal gas relationship (ref. 8):

$$M_\infty = \left[\frac{1}{\epsilon}\left(\frac{2}{\gamma - 1}\right)\left(\frac{T_o}{T_\infty} - 1\right)\right]^{1/2}$$

in which ϵ is the recovery factor of the total-temperature probe and equals 0.994, T_o is the total temperature sensed by the probes, and T_∞ is the ambient temperature.

Ambient temperature, T_∞, was obtained by correlating the pressure altitude measured on the XB-70 airplane with rawinsonde-measured pressure altitudes.

Wind-Tunnel Tests

A large portion of XB-70 flights at Mach numbers greater than 2.5 were at ground distances of 160 kilometers (100 miles) or more from the radar site and at altitudes near 21,000 meters (70,000 feet). As a result, uncertainties in the flight data due to the low ambient pressures and the low radar elevation angles were greater than for flights at lower altitudes and Mach numbers. Wind-tunnel data were obtained for both XB-70 pitot-static probes to supplement the flight data. The tests were made in the NASA Langley Research Center's Unitary Plan wind tunnel (ref. 9) at several simulated flight altitudes and at flight Mach numbers of 2.60, 2.80, and 2.96.

PRECISION

A variety of sensors and support equipment was needed for the three airspeed methods used. In this section the errors of the individual sensors and supporting equipment are discussed and a root-sum-squared error is presented for each method.

Uncertainties in Sensors and Supporting Equipment

Pacer. – For most of the Pacer data, the altimeter system of the Pacer airplane had an estimated uncertainty of ±15 meters (±50 feet) (ref. 10) over an altitude range of 9100 meters (30,000 feet) to 12,000 meters (40,000 feet).

Pressure transducers. – Laboratory tests indicated the overall accuracy of the pressure transducers to be ±0.05 percent of the full-scale range of the pressure cell. The static-pressure cell had a range of 0 to 138×10^3 newtons/meter^2 (0 to 20 pounds/inch^2); its accuracy would therefore be ±69 newtons/meter^2 (±0.010 pound/inch^2). The stagnation-pressure cell range was from 0 to 207×10^3 newtons/meter^2 (0 to 30 pounds/inch^2) with an accuracy of ±103 newtons/meter^2 (±0.015 pound/inch^2). An aneroid barometer with a range of 60.96 centimeters to 78.74 centimeters (24 inches to 31 inches) of mercury was used for preflight and postflight zero corrections to the

transducer-measured pressures. The accuracy of this split-range barometer was estimated to be ±0.02 centimeter (±0.01 inch) of mercury. Figure 8 shows the uncertainty in Mach number and altitude corresponding to the combined inaccuracies in the pressure-measuring system used on the XB-70 airplane to obtain airspeed data.

Radar (AN/FPS-16).– The pointing accuracy of the AN/FPS-16 radar complex used to obtain height information was estimated to be $\pm 1.964 \times 10^{-4}$ radians (±0.2 mil). Figure 9 illustrates the resultant uncertainty in radar-measured geometric altitudes. As shown, this altitude uncertainty increased with decreasing elevation angle for any given altitude.

AN-GMD-1 (AN/AMT-4B) rawin set.– Ambient pressures and temperatures were obtained from a combination of an AN/AMT-4B rawinsonde balloon and an AN/GMD-1 rawin set. The uncertainties in the pressure measurements varied from ±1.2 millibars at an altitude of 9100 meters (30,000 feet) to ±0.40 millibar at an altitude of 21,000 meters (70,000 feet). The accuracy of the measured ambient air temperature was ±0.7° C (±1.3° F) for the entire altitude range (ref. 11).

Total-temperature probe.– Many variables must be considered (ref. 12) in assessing the errors involved in calculating Mach number from total-temperature-probe measurements. Four of the primary error sources are self-heating, calibration, recovery factor, and radiation (ref. 13). The magnitudes of these errors were estimated for the total-temperature probe for an altitude of 18,000 meters (60,000 feet) and a Mach number of 3.0 (ref. 13). From the types of errors discussed in reference 13, a total root-sum-squared uncertainty of ±0.44° C (±0.8° F) was calculated as the total-temperature uncertainty. In addition to the basic error associated with the total-temperature probe, the aircraft's wiring, amplifiers, indicators, and recorders introduced errors. Ground calibration checks on the XB-70 airplane indicated that the combination of the probes and the support system resulted in a total-temperature error of ±2.8° C (±5° F) at temperatures near 315° C (600° F), which is within the specified tolerance of 1 percent for the entire system.

Uncertainties in the Flight Calibration Procedures and Wind-Tunnel Data

Pacer method.– Pacer data from several flights indicated a Mach number measurement uncertainty of ±0.002. This uncertainty existed over the subsonic Mach number range and for altitudes below 11,000 meters (35,000 feet).

Acceleration-deceleration radar method.– The Mach number and altitude uncertanties that resulted from the apparent errors in the various sensors and support equipment were determined by using a root-sum-squared equation. These uncertainties for the entire flight Mach number range are presented in figure 10 for two calibration procedures, one in which the reference pressures were determined from the Pacer system, and the other in which they were determined from a combination of a radar and a rawinsonde balloon. The uncertainties were larger when the rawinsonde system was used than when the Pacer system was used. It was noted that the magnitude of the scatter in the flight data for both methods was close to the predicted scatter presented in figure 10 throughout the Mach number range.

The equations used to derive the error in Mach number due to the error in the

instrumentation system are presented in reference 14.

Total-temperature method.– The total-temperature method for determining true Mach number is subject to error from several sources. To estimate the error in calculating Mach number by this method the uncertainties in three basic parameters are used: (1) ambient temperature, which is found by relating aircraft indicated pressure altitude to rawinsonde pressure altitude; (2) total temperature; and (3) specific-heat ratio. An uncertainty of ±0.01 in the specific-heat ratio may exist at a Mach number of approximately 3.0 and at altitudes of 18,000 meters (60,000 feet) to 24,000 meters (80,000 feet) (ref. 13).

The resulting uncertainty for a Mach number of 3 and a geometric altitude of 18,000 meters (60,000 feet) was calculated by using the relationship (ref. 15)

$$\text{Mach number uncertainty} = \sqrt{\left(\frac{\partial M_\infty}{\partial T_\infty}\Delta T_\infty\right)^2 + \left(\frac{\partial M_\infty}{\partial T_o}\Delta T_o\right)^2 + \left(\frac{\partial M_\infty}{\partial \gamma}\Delta\gamma\right)^2}$$

in which the uncertainties are: T_o, ±2.78° C (±5° F); T_∞, ±0.72° C (±1.3° F); and γ, ±0.01 for a total temperature of 333° C (633° F). The Mach number uncertainty was calculated to be ±0.05. This is close to the scatter in the total-temperature-probe data calculated for a Mach number of approximately 3 and a geometric altitude of approximately 21,000 meters (70,000 feet). The scatter in the data from eight XB-70 flights indicated that the errors in the total-temperature-probe method were:

Mach number	Altitude, m (ft)	Uncertainty in Mach number
1.5	9000 (30,000)	±0.01
2.5	12,000 to 18,000 (40,000 to 60,000)	±0.02
3.0	18,000 to 21,000 (60,000 to 70,000)	±0.04

Wind-tunnel data.– Pressure measurements were made in the Langley Unitary Plan wind tunnel with several different pressure sensors: two quartz pressure gages, four variable-range pressure cells, two mercury manometers, and several differential-pressure transducers. The instrumentation used for the XB-70 pitot-static probes was also used for free-stream pitot- and static-pressure measurements in the wind-tunnel-test section. Estimated uncertainties in measurements corresponded to Mach number uncertainties of ±0.005 for most of the probe calibration test points. For the lowest test pressure and Reynolds number the uncertainties were no more than ±0.01.

TESTS

Figure 11 shows regions of comparable flight- and wind-tunnel-test data. All the wind-tunnel data presented in this report were averaged for each specific test condition,

and are for zero angle of sideslip. The flight data obtained for level flight conditions were used to establish the position-error calibration when radar elevation angles were larger than 5° and the ground distances from radar to aircraft were less than 161 kilometers (100 miles). Because all the data used were selected from steady-state (constant-altitude) flight conditions, pressure lag could be discounted as a source of error in position-error determination. Most of the higher supersonic data were obtained in the altitude range between 15,000 meters (50,000 feet) and 21,000 meters (70,000 feet). The angles of attack of the pitot-static probe and nose boom were approximately -2° for most of the supersonic data points.

RESULTS AND ANALYSIS

XB-70 Position Errors From Wind Tunnel and Flight

Preliminary analysis of the Langley Research Center wind-tunnel data for the compensated pitot-static probe indicated that Reynolds number was important in determining position error. In addition to the Reynolds number effect, angle-of-attack and shock-wave boundary-layer interaction on the pitot-static probe influenced the position error and could be isolated only from the wind-tunnel-test data. Figure 12(a) shows that the position errors calculated from the flight and wind-tunnel data show close agreement for similar values of Reynolds number and angle of attack (-2°) at a Mach number of 2.60. This agreement firmly established the magnitude level for the position error at Mach 2.60. The wind-tunnel data at Mach 2.80 and 2.96 were also plotted and faired (figs. 12(b) and 12(c)). However, some extrapolation was necessary because the Reynolds numbers for the wind-tunnel data at Mach 2.80 and 2.96 were not comparable in magnitude to the flight Reynolds number. In extrapolating the data, the general shapes of the fairings were taken from figure 12(a).

Figure 12 also shows that the error in the compensated probe at Mach numbers from 2.60 to 2.96 decreases as the probe angle of attack increases from -2° to 2°. For example, indicated errors at flight Reynolds numbers are large at $\alpha = -2°$, moderate at $\alpha = 0°$, and small for $\alpha = 2°$. This trend is of practical significance because of the large errors experienced at flight angles of attack near -2°. The large flight position errors could have been greatly reduced if probe angles of attack had been near 2°. This could have been assured if the XB-70 nose boom had been installed parallel to the aircraft's centerline instead of drooped 4.17° (fig. 4).

The aircraft's fuselage flow field forward of the nose produced a large position error in the subsonic and transonic Mach number ranges. In addition, part of the position error was introduced in the transonic Mach number range by the nose boom (fig. 4) which affected the pitot-static measurements (ref. 16, page 89). Isolation of the support effects from the forebody effects was not attempted. A normal shock at the pitot-static-probe tip, together with a supersonic flow field around the static orifices on the probe, was the main source of the supersonic position error. Therefore, in this analysis the position-error calibrations are divided into subsonic and supersonic parts.

Figure 13 presents airspeed data obtained on several XB-70 flights on which the

uncompensated and compensated probes were used in the S_1/S_2 configuration. The position error was determined by using the Pacer, radar acceleration-deceleration, and total-temperature methods. These data are faired in figure 14(a) and compared with wind-tunnel data in the Mach number range from 2.6 to 2.96. The difference between the extrapolated wind-tunnel data of figure 12 and the faired flight data of figure 14(a) is small. Equivalent curves in terms of $\frac{\Delta p}{p_\infty}$ and Δh versus indicated Mach number are plotted in figures 14(b) and 14(c), respectively. The position-error fairings, presented in figure 14(a), were made through flight data which were selected for optimum conditions of accuracy. For the higher supersonic Mach number portion of the fairing, the wind-tunnel data were used in conjunction with limited flight data in establishing the final curve. The uncertainties in the final fairing (fig. 14(a)) were:

M_∞	h_r, m (ft)	Position-error uncertainty
0.5 to 1.4	9000 (30,000)	±0.002
1.4 to 2.5	9000 (30,000) to 18,000 (60,000)	±0.005
2.5 to 3.0	18,000 (60,000) to 21,000 (70,000)	±0.01

Subsonic.– At Mach numbers less than 1.0 the position error of the uncompensated pitot-static probe showed the expected increase due to the increase in the pressure field ahead of the aircraft as the Mach number increased. The compensated probe, which was designed to eliminate the effects of this pressure field, tended to overcorrect in the subsonic region. This overcorrection became larger at the higher Mach numbers and reached a maximum value of $\Delta M = 0.01$; however, at landing speed the correction was nearly zero. As a result, the pressures measured by the compensated probe were below ambient, whereas the uncompensated probe indicated pressures above ambient (fig. 14(b)). For a comparison at an indicated Mach number of 0.960 and an altitude of 9750 meters (32,000 feet), the ΔM and Δh errors of the uncompensated probe were 0.054 and 408 meters (1340 feet), respectively, whereas the compensated probe for the same flight conditions had a ΔM error of -0.0095 and a Δh error of 70 meters (233 feet).

Supersonic.– Near Mach 1 the bow shock wave of the aircraft passed over the static orifices, and the high-pressure flow field around the aircraft was no longer sensed by the pitot-static probe. Immediately after the bow shock wave passed, the measured pressures from the compensated probe dropped further below ambient pressure (fig. 14(b)). With increasing Mach numbers, the pressures sensed by the compensated probe approach ambient pressure near a Mach number of 1.3 and drop rapidly below the ambient pressure for Mach numbers greater than 1.3. Consequently, the calibration curve for the compensated pitot-static probe (fig. 14) indicates Mach numbers and altitudes that are always higher than true values ($M_i > 1$).

For Mach numbers from 1 to approximately 2.2, the uncompensated pitot-static probe indicated pressures higher than ambient pressure (indicated Mach number and

altitude lower than true Mach number and altitude). Above approximately Mach 2.2, the uncompensated probe exhibits a trend similar to that of the compensated probe; namely, an increasingly larger negative position error (indicated Mach number and altitude higher than true Mach number and altitude) with increasing Mach number. For example, at an indicated Mach number of 2.6, the compensated and uncompensated pitot-static probes indicated Mach numbers higher than true values by 0.061 and 0.027, respectively. Values of ΔM and $\frac{\Delta p}{p_\infty}$ for figure 14 are listed in table 1.

Analysis of Pitot-Static-Probe Characteristics

Angle-of-attack sensitivity.– Analysis of the wind-tunnel data from the Langley Research Center showed that the compensated and uncompensated pitot-static probes were both sensitive to angle-of-attack variations when angle of attack was less than 0°. For example, from figure 15, for a negative angle of attack, the calculated rate of change in Mach number position error per degree of angle-of-attack change (sensitivity) was approximately 0.02 for both probes. For positive angles of attack up to 8°, the wind-tunnel data show that sensitivity to angle-of-attack changes is reduced. The uncompensated probe shows the greatest sensitivity reduction to -0.002, whereas the compensated probe is 0.01.

The sensitivity of the NACA A-6 pitot-static probe (ref. 17) is compared with the sensitivities of both XB-70 pitot-static probes in figure 15. For negative angles of attack the sensitivity of the A-6 probe is only -0.005 and becomes negligible for positive angles of attack. This insensitivity to changes in angle of attack results from the probe construction. The probe was built with the top and bottom static orifices manifolded together (fig. 16(a)), whereas the static orifices of both XB-70 probes were located only on the bottom (figs. 16(b) and (c)). Figure 16 also shows the construction of the pitot openings for all three probes. The sensitivity of the XB-70 probes to negative angles of attack is consistent with that of other probes with static orifices on the bottom.

Reynolds number effect.– Figures 17(a) and 17(b) show the effects of Reynolds number variation on the compensated and the uncompensated XB-70 pitot-static probes. At negative angles of attack the wind-tunnel data indicate that the cylinder-shaped uncompensated probe was less affected by Reynolds number variations than the compensated probe. Effects of Reynolds number variation on the NACA cylindrical pitot-static probe at large angles of attack were noted in reference 17. For all three probes, the wind-tunnel data show that as the Reynolds number increases, the static-pressure error becomes more positive. Data from references 16 and 17 also indicate that variations in pressure measured on pitot-static probes may be dependent on Reynolds number changes.

Reynolds number effects on pitot-static-probe stagnation-pressure measurements (refs. 18 to 20) and boundary-layer effects on the pitot-static probes (refs. 20 and 21) were demonstrated in previous tests. Figure 18 is a composite drawing from four wind-tunnel shadowgraphs taken of the XB-70 compensated pitot-static probe at $M_\infty = 2.6$ and angles of attack of -5° and 4°. The drawings graphically illustrate the transition from a turbulent to a laminar boundary layer over the static orifices on the compensated pitot-static probe as Reynolds number is reduced. It is apparent that a turbulent boundary layer exists over most of the compensated probe for a high Reynolds

number (fig. 18(a)). At a lower Reynolds number the boundary layer is laminar around the static ports and becomes turbulent only on the small neck of the probe (fig. 18(b)). A similar trend occurred at an angle of attack of 0°. Such in-flight boundary-layer changes on pitot-static probes make airspeed calibrations difficult to obtain.

Comparison of static-orifice location on the compensated probe.– The compensated pitot-static probe (figs. 3 and 16(b)) also had a set of uncompensated static orifices (S_3). A limited amount of data from the S_3 orifices was analyzed and is presented in figure 19. Subsonic and supersonic data from the uncompensated static ports (S_3) were compared with the data from the S_1/S_2 orifices on the uncompensated pitot-static probe. The S_3 data fall below the fairing for the uncompensated probe for all subsonic Mach numbers. For supersonic Mach numbers the pressures measured at the S_3 orifices were closer than the S_1/S_2 data to ambient pressure. Therefore, the ΔM points are close to zero for $M_i \approx 1.2$ (fig. 19).

Figure 19 also compares the S_3 orifice data and data taken from the compensated orifices on the same probe. This illustrates the dissimilar types of position-error curves which can be obtained when one set of static orifices is placed on the compensated portion of the probe and another set is placed on the uncompensated portion, separated by 2.54 centimeters (1 inch).

Comparison of position errors.– Figure 20 compares position errors for several types of pitot-static probes. The position-error curves were obtained from theory, wind-tunnel tests, and flight data. To eliminate forebody effects, only supersonic data were analyzed. For Mach numbers greater than 1, modified slender-body theory (ref. 16) was applied for the cylindrical, uncompensated XB-70 pitot-static probe. The theory predicts that static orifices on cylindrical probes will sense static pressures which are higher than ambient pressure, and that therefore the indicated Mach numbers will be less than the true Mach numbers (ΔM will be positive). Data from the XB-70 uncompensated probe and the NACA A-6 (ref. 22) pitot-static probes tend to confirm this theory up to a Mach number of approximately 2. Above this Mach number both XB-70 probes and the A-6 probe sensed static pressures which were less than ambient pressure; hence, ΔM became negative. Therefore, indicated Mach numbers are greater than true Mach numbers for these types of pitot-static probes. The position error of the A-6 probe increases most rapidly at Mach numbers greater than 2, possibly because of the strong normal shock in front of its blunt tip.

The compensated probe with static orifices on the rear noncylindrical surface sensed pressures which were below ambient for all Mach numbers greater than 1 and showed a negative position error for all supersonic Mach numbers tested.

Also shown in figure 20 are data from a compensated probe (ref. 23) with static orifices on the forward tapered tip. Data from this probe indicated pressures higher than ambient between Mach 1 and 2. Limited wind-tunnel data (ref. 24) indicate that this could also be true for Mach numbers greater than 2.

Influence of Pitot-Static Probes on Supersonic Transport Operation and Performance

Selection of a pitot-static probe for a supersonic cruise aircraft could present a problem. A compensated probe would reduce the unwanted transonic errors, but could introduce undesirable Reynolds number and angle-of-attack effects at supersonic speeds. An uncompensated probe would have large subsonic position errors but smaller errors at supersonic speeds. In addition, it would be less susceptible to Reynolds number and angle-of-attack variation at supersonic speeds. Therefore, for a supersonic cruise vehicle, a pitot-static probe with both compensated and uncompensated sets of orifices would appear to be desirable. This type of probe would have a minimum position error at subsonic and supersonic speeds and would therefore provide better utilization of airspace than a conventional pitot-static probe. The general guidelines for designing such a probe are given in reference 25. The design of the uncompensated section could be similar to that of the static-orifice section on the NACA A-6 probe.

Reliable air data are needed not only by the pilot and for control systems but also because air data errors and uncertainties affect the performance and operational characteristics of an aircraft. For example, if the two probes tested on the XB-70 airplane were used on a supersonic transport and the transonic and supersonic errors were not accounted for, the altitude errors for typical subsonic and supersonic cruise conditions would be:

Cruise condition		Altitude error, km (ft)	
Mach number	Altitude, km (ft)	Compensated probe	Uncompensated probe
2.70	21.3 (70,000)	±0.30 (±1000)	±0.17 (±550)
2.00	16.8 (55,000)	±.21 (±700)	±.06 (±200)
.90	12.2 (40,000)	±.05 (±180)	±.24 (±800)

Errors of these magnitudes would make it difficult or impossible to comply with the minimum vertical height separations required by typical commercial flight regulations (ref. 26). In addition, the Mach number errors of the two types of pitot-static probes could have great effect on the control system of a supersonic transport inlet. If the pitot-static system were used as an input to the inlet control and the corrections to the air data parameters were not made, the inlet would not be controlled to the optimum setting for peak recovery. The magnitude of the errors in inlet recovery that could be caused by the Mach number position errors of the compensated and uncompensated probes is shown in figure 21 together with typical supersonic transport inlet recovery curves (ref. 27). It is assumed that the transport inlet would be scheduled to operate according to the nominal line, which is approximately 3 percent below the level where inlet instability would occur. Figure 21 shows that if the inlet were scheduled by air data information from either of the two probes, the inlet control would cause inlet instability at Mach 2.15 for the compensated probe and Mach 2.75 for the uncompensated probe. If an inlet requires a control input from a pitot-static system, knowledge of the position error of the probes would eliminate one source of error.

CONCLUDING REMARKS

A compensated and an uncompensated pitot-static probe, used on the XB-70 airplane, were calibrated in flight over a Mach number range from low subsonic to supersonic (near 3). The calibration methods, probe behavior, and probe characteristics were compared. It was found that the position error of the compensated pitot-static probe at subsonic speeds was much less than that of the uncompensated probe. For example, the absolute maximum subsonic Mach number position error measured by the uncompensated pitot-static probe was 0.054, whereas the compensated probe indicated an absolute maximum of only 0.01.

At supersonic speeds the compensated pitot-static probe indicated an increasingly negative position error with increasing Mach number. The uncompensated probe had small positive position errors below a Mach number of 2.2 and increasingly larger negative position errors at Mach numbers greater than 2.2. For example, at an indicated Mach number of 2.6, the compensated and uncompensated pitot-static probes indicated Mach numbers higher than true values by 0.061 and 0.027, respectively.

For supersonic conditions, the compensated pitot-static probe was more sensitive than the uncompensated probe to Reynolds number and angle-of-attack effects. To obtain the most repeatable airspeed data the pitot-static probes should be flown at a small positive angle of attack. Comparison of both of the XB-70 pitot-static probes with an NACA A-6 pitot-static probe showed the latter to be less sensitive to angle-of-attack variations.

The level acceleration-deceleration method of obtaining airspeed calibrations proved to be satisfactory for obtaining precision airspeed data over a large Mach number range. This technique minimized the test support requirements and reduced inherent lag problems.

This study indicated that a pitot-static probe with both a compensated and an uncompensated set of static orifices should be used for supersonic transports. This type of probe would have a minimum position error at subsonic and supersonic speeds and would therefore provide better utilization of airspace and inlet performance than a conventional pitot-static probe.

Flight Research Center,
National Aeronautics and Space Administration,
Edwards, Calif., December 30, 1971.

REFERENCES

1. DeLeo, Richard V.; and Hagen, Floyd W.: Development of Aerodynamically Compensated Pitot-Static Tubes for Use on the XB-70 Aircraft. Tech. Doc. Rep. No. RTD-TDR-63-4085, Research and Technology Div., Air Force Systems Command, Wright-Patterson Air Force Base, Ohio, 1963.

2. Mechtly, E. A.: The International System of Units - Physical Constants and Conversion Factors. NASA SP-7012, 1969.

3. Edwards, E. L.: An Airborne Data Acquisition System for Use in Flight Testing the XB-70 Airplane. Selected Instrumentation Application Papers From AGARD Flight Mechanics Panel - Twenty-Sixth Meeting, AGARD Rep. 507, June 1965, pp. 23-48.

4. Anon.: Radiosondes AN/AMT-4A and AN/AMT-4B. TM 11-2432A to 31M4-2AMT4-11, Depts. of Army and Air Force, June 1958. (Supersedes TM 11-2432A.)

5. Anon.: Manual of Radiosonde Observations (WBAN). Circular P, seventh ed., U.S. Weather Bur., U.S. Air Force, U.S. Navy, June 1957.

6. Daniel, O. H.: Electronic Computer Reduction of Upper Air Data. 4WG Pamphlet No. 105-7-2, 4th Weather Group, Air Weather Service (MATS), U.S. Air Force, June 1961.

7. Herrington, Russel M.; Shoemacher, Paul E.; Bartlett, Eugene P.; and Dunlap, Everett W.: Flight Test Engineering Handbook. Tech. Rep. No. 6273, Air Force Flight Test Center, May 1951 (rev. Jan. 1966).

8. Dommasch, Daniel O.; Sherby, Sydney S.; and Connolly, Thomas F.: Airplane Aerodynamics. Fourth ed., Pitman Publishing Corp., 1967, p. 62.

9. Schaefer, William T., Jr.: Characteristics of Major Active Wind Tunnels at the Langley Research Center. NASA TM X-1130, 1965, p. 32.

10. De Anda, Albert G.; and Curtis, Lawrence C., Jr.: F-104 Airspeed System Calibrations. FTC-TR-66-35, Air Force Flight Test Center, 1966.

11. Anon.: Meteorological Equipment Data Accuracies. Doc. IRIG-110-64, Meteorological Working Group, Inter-Range Instrumentation Group (IRIG), Mar. 1965. (Available from DDC as AD 467152.)

12. Woodfield, A. A.; and Haynes, P. J.: Measurement of Air Temperature on an Aircraft Travelling at High Subsonic and Supersonic Speeds. C. P. No. 809, Ministry of Aviation, British A.R.C., 1965.

13. DeLeo, Richard V.; Cannon, Peter J.; and Hagen, Floyd W.: Evaluation of New Methods for Flight Calibration of Aircraft Instrument Systems. TR-59-295, Part I, Wright Air Development Center, June 1959. (Available from DDC as AD 239767.)

14. Zalovcik, John A.: A Radar Method of Calibrating Airspeed Installations on Airplanes in Maneuvers at High Altitudes and at Transonic and Supersonic Speeds. NACA Rep. 985, 1950.

15. Beers, Yardley: Introduction to the Theory of Error. Second ed., Addison-Wesley Publishing Co., Inc., 1962.

16. Hill, J. A. F.; Baron, J. R.; Schindel, L. H.; and Markham, J. R.: Mach Number Measurements in High-Speed Wind Tunnels. AGARDograph 22, Oct. 1956.

17. Richardson, Norman R.; and Pearson, Albin O.: Wind-Tunnel Calibrations of a Combined Pitot-Static Tube, Vane-Type Flow-Direction Transmitter, and Stagnation-Temperature Element at Mach Numbers From 0.60 to 2.87. NASA TN D-122, 1959.

18. Wuest, Walter: Pressure Measuring Probes in Aerodynamic Research Technology. Proceedings of the First Meeting of the Subcommittee on Aerodynamic Measuring Technology, NASA TT F-11856, Jan. 1969, p. 41.

19. Macmillan, F. A.: Viscous Effects on Pitot Tubes at Low Speeds. J. Roy. Aeron. Soc., vol. 58, 1954, p. 570.

20. Holder, D. W.; North, R. J.; and Chinneck, A.: Experiments with Static Tubes in a Supersonic Airstream. Parts I and II, R. & M. No. 2782, British A.R.C., July 1950.

21. Matthews, Malcolm L.: An Experimental Investigation of Viscous Effects on Static and Impact Pressure Probes in Hypersonic Flow. Memorandum No. 44, Calif. Inst. Technol., June 2, 1958.

22. Larson, Terry J.; and Webb, Lannie D.: Calibrations and Comparisons of Pressure-Type Airspeed-Altitude Systems of the X-15 Airplane From Subsonic to High Supersonic Speeds. NASA TN D-1724, 1963.

23. Carrillo, J. G.: Flight Calibration of the F-104 Compensating Airspeed Head. Rep. No. 16959, Lockheed Aircraft Corporation, June 1963.

24. Hess, J. L.; and Smith, A. M. O.: Static-Pressure Probes Derived from Supersonic Slender-Body Theory. J. Aircraft, vol. 4, no. 5, Sept.-Oct. 1967, pp. 409-415.

25. Ritchie, Virgil S.: Several Methods for Aerodynamic Reduction of Static-Pressure Sensing Errors for Aircraft at Subsonic, Near-Sonic, and Low Supersonic Speeds. NASA TR R-18, 1959.

26. Anon.: Federal Aviation Regulations. Parts 91.109 and 91.121—General Operating and Flight Rules. FAA, Sept. 30, 1963.

27. Koenig, Robert W.: Inlet Sensitivity Study for a Supersonic Transport. NASA TN D-3881, 1967.

TABLE 1.– VALUES OF ΔM AND $\frac{\Delta p}{p_\infty}$ CALIBRATION FOR THE COMPENSATED AND UNCOMPENSATED PROBES

[S_1/S_2 configuration]

M_i	Compensated probe		Uncompensated probe	
	ΔM	$\frac{\Delta p}{p_\infty}$	ΔM	$\frac{\Delta p}{p_\infty}$
0.50	-0.0016	-0.0011	0.0125	0.0085
.60	-.0018	-.0014	.0155	.0124
.70	-.0027	-.0024	.0195	.0178
.80	-.0045	-.0044	.0245	.0249
.85	-.0064	-.0066	.0285	.0304
.90	-.0080	-.0086	.0355	.0396
.93	-.0088	-.0097	.0425	.0487
.96	-.0095	-.0107	.0540	.0635
.99	-.0098	-.0113	.0300	.0354
1.00	-.0100	-.0116	.0235	.0278
1.01	0	0	.0040	.0047
1.05	-.03	-.0354	.0050	.0060
1.10	-.0225	-.0271	.0065	.0079
1.20	-.0160	-.0194	.0095	.0115
1.30	-.0137	-.0163	.0125	.0147
1.40	-.0145	-.0167	.0145	.0166
1.50	-.0175	-.0195	.0163	.0179
1.60	-.0205	-.0220	.0175	.0185
1.70	-.0245	-.0253	.0180	.0183
1.80	-.0284	-.0282	.0175	.0171
1.90	-.0322	-.0308	.0148	.0139
2.00	-.0362	-.0333	.0110	.0099
2.10	-.0402	-.0356	.0062	.0054
2.20	-.0440	-.0376	.0015	.0013
2.30	-.0483	-.0398	-.0050	-.0041
2.40	-.0525	-.0418	-.0120	-.0094
2.50	-.0568	-.0436	-.0195	-.0148
2.60	-.0614	-.0456	-.0270	-.0198
2.70	-.0660	-.0475	------	------
2.80	-.0713	-.0497	------	------
2.90	-.0773	-.0523	------	------
3.00	-.0832	-.0546	------	------
3.10	-.0900	-.0574	------	------
3.20	-.0985	-.0611	------	------

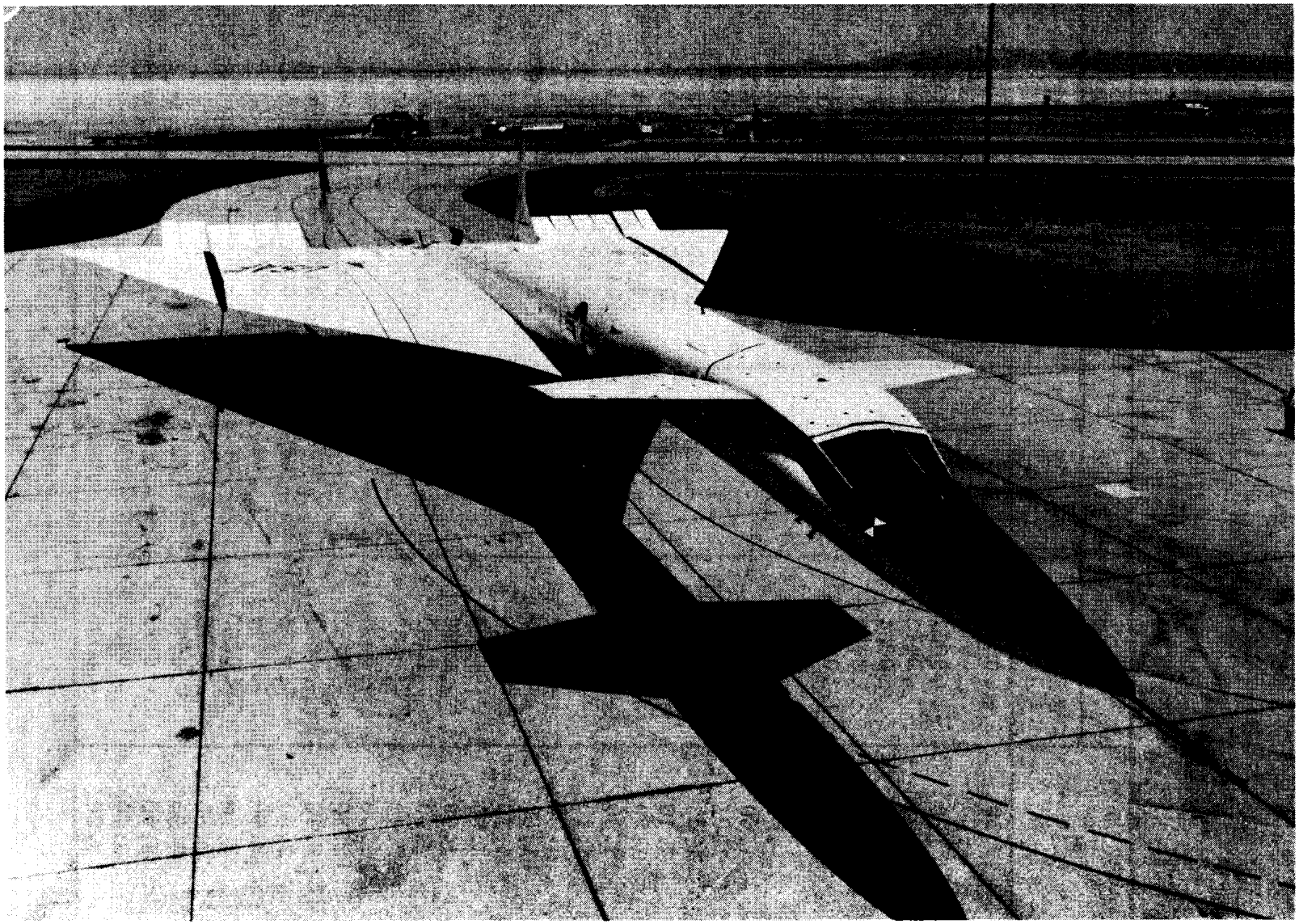

ECN-1814

Figure 1. XB-70 airplane.

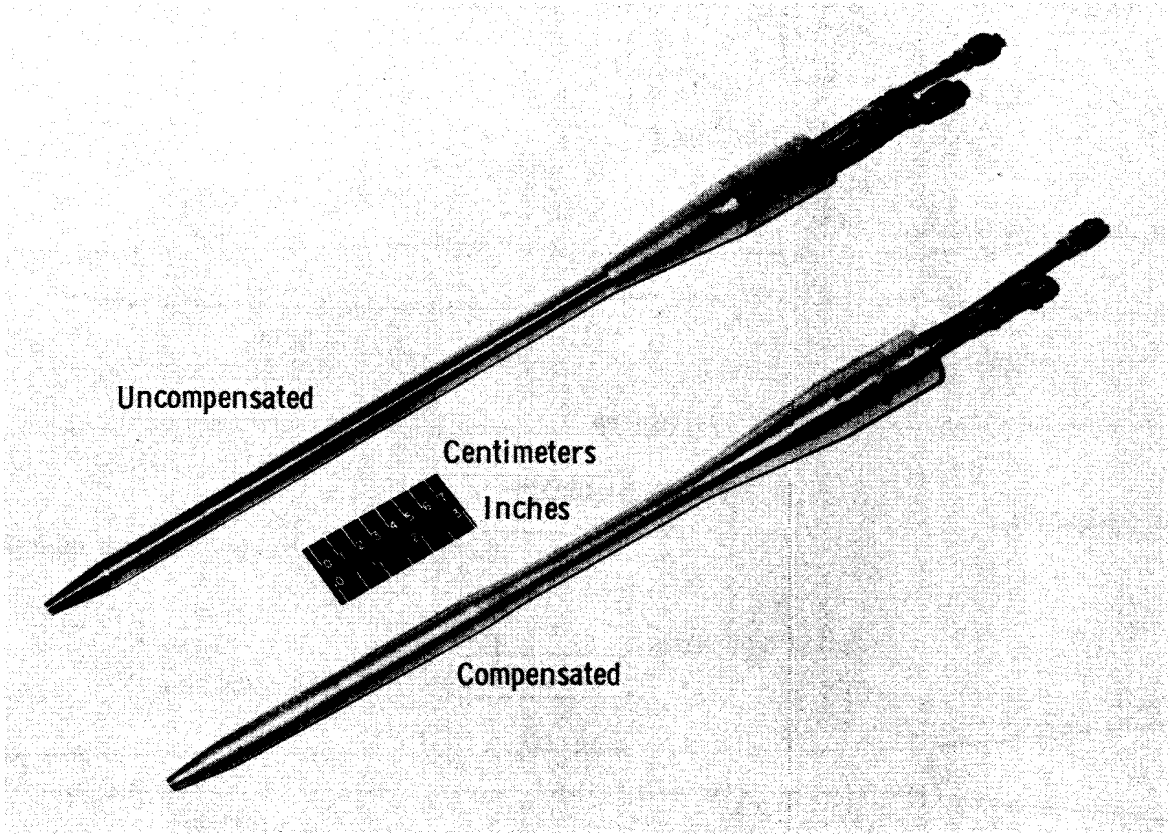

E-21219

Figure 2. XB-70 compensated and uncompensated pitot-static (airspeed) probes.

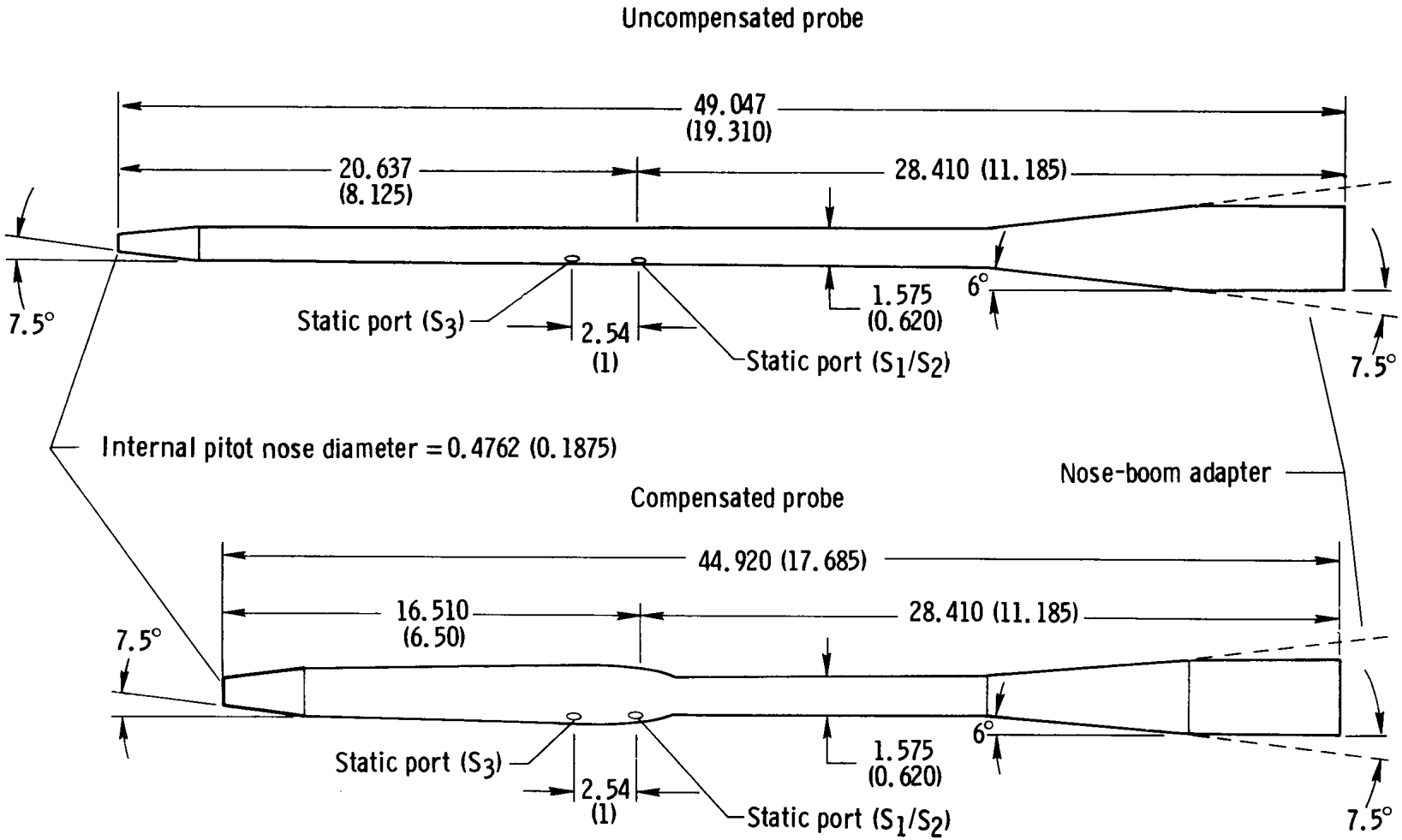

Figure 3. Details of the compensated and uncompensated pitot-static airspeed probes used on the XB-70 aircraft. Dimensions in centimeters (inches) unless otherwise noted.

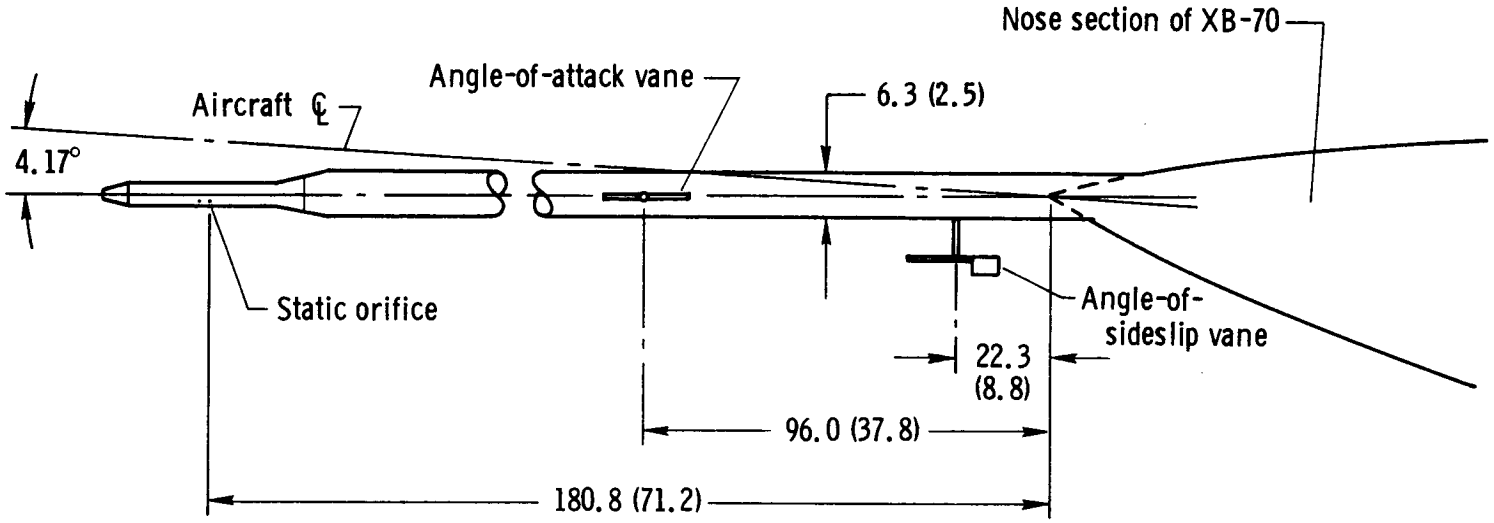

Figure 4. Sketch of the nose boom showing the location of the pitot-static probe (either uncompensated or compensated), angle-of-attack vane, and angle-of-sideslip vane. Dimensions in centimeters (inches) unless otherwise noted.

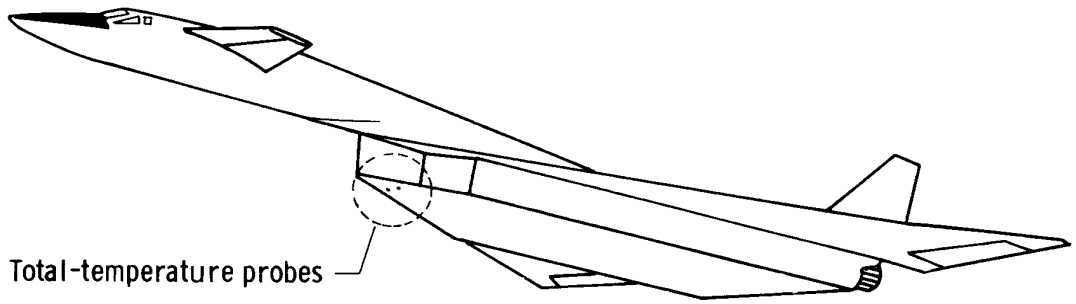

(a) Location of probes.

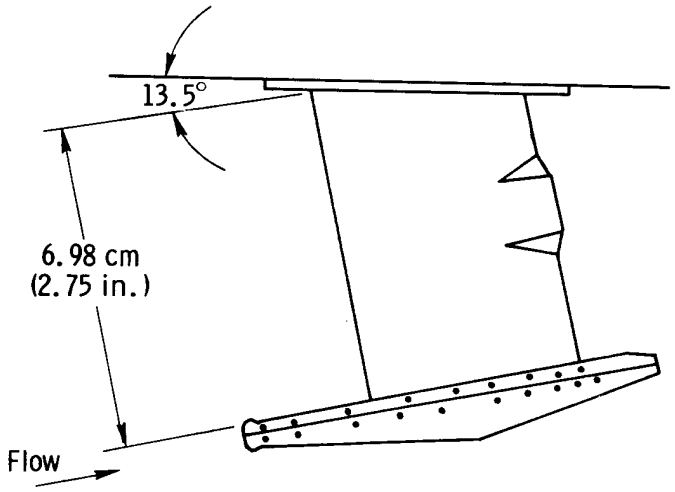

(b) Sketch of probe showing dimensions.

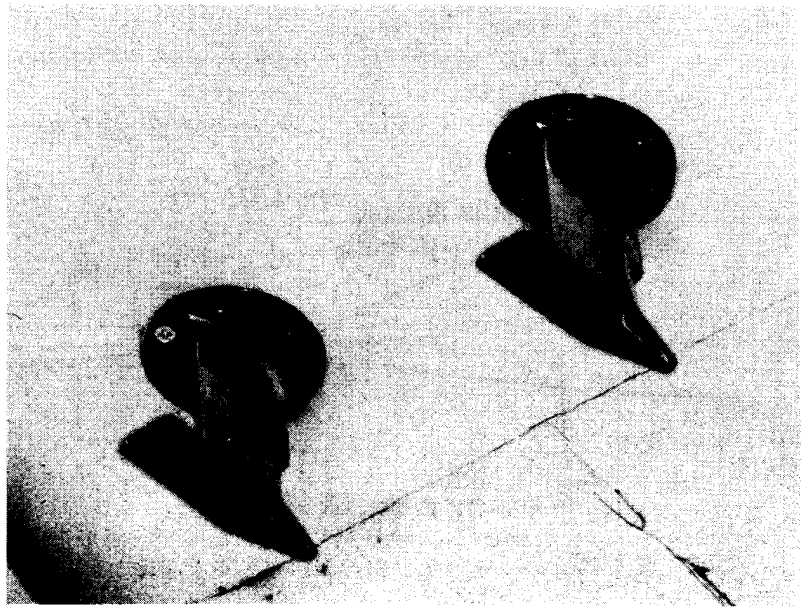

(c) Photograph of both probes.

Figure 5. Sketches and photograph of the two XB-70 total-temperature probes.

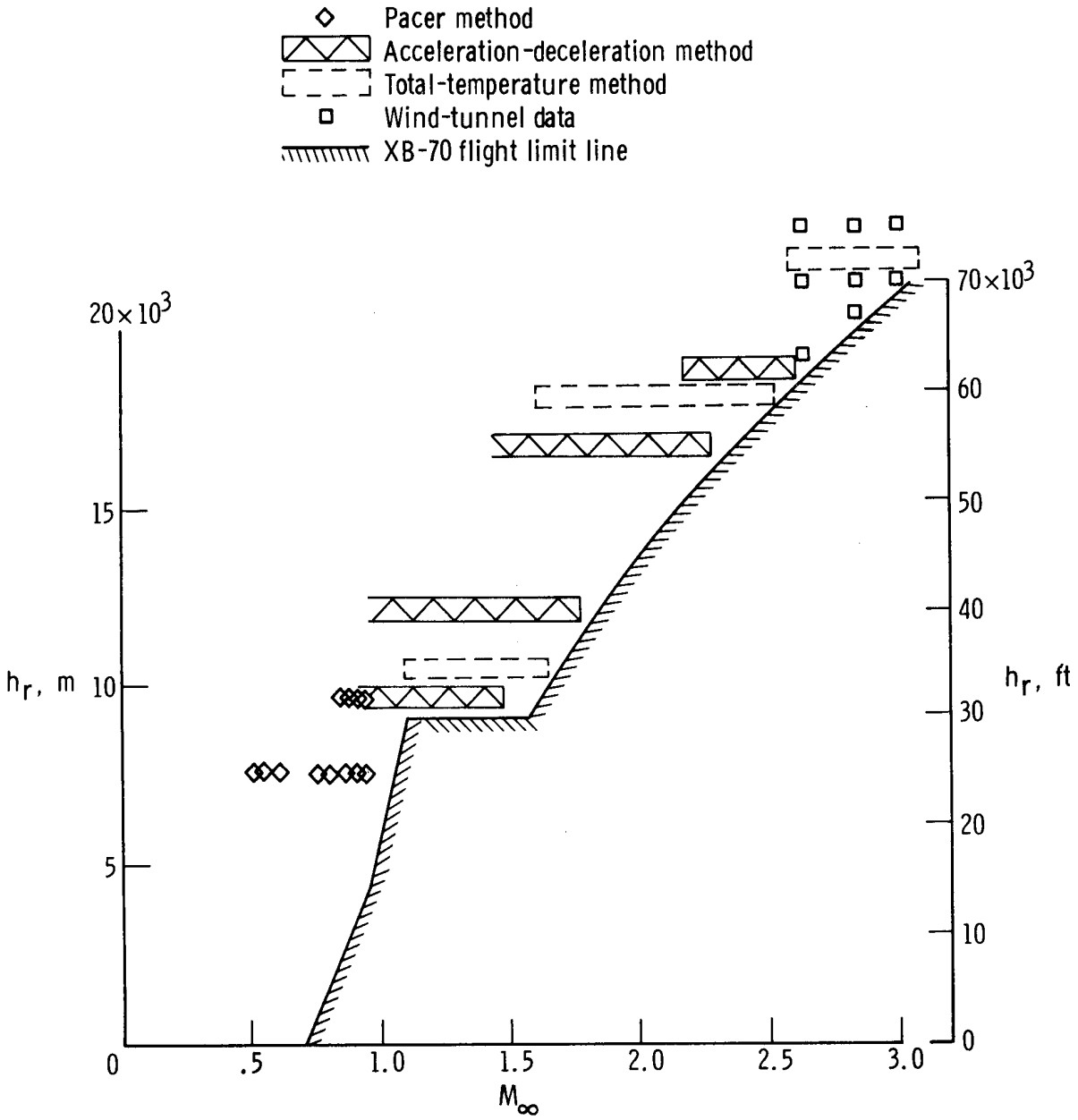

Figure 6. Flight envelope showing the flight regions in which various methods were used to obtain the XB-70 airspeed calibration.

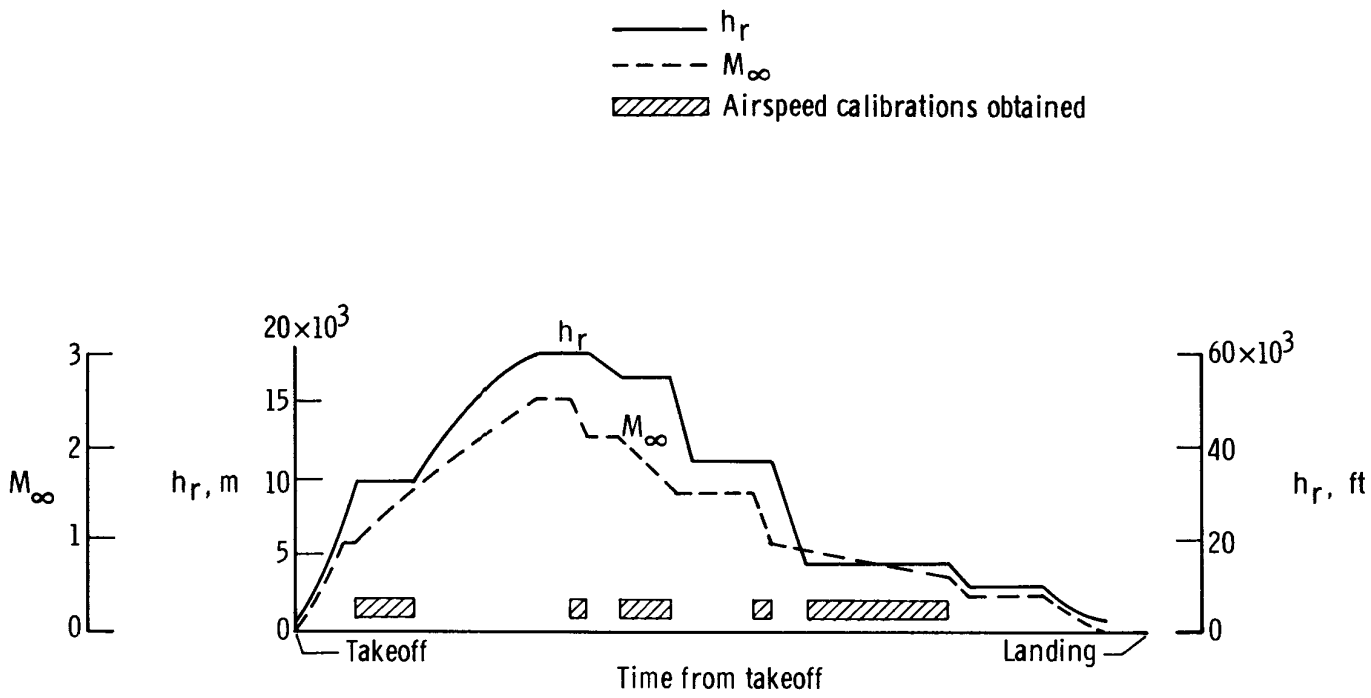

Figure 7. Typical XB-70 Mach number and altitude time history showing time segments during which acceleration-deceleration airspeed calibrations were obtained.

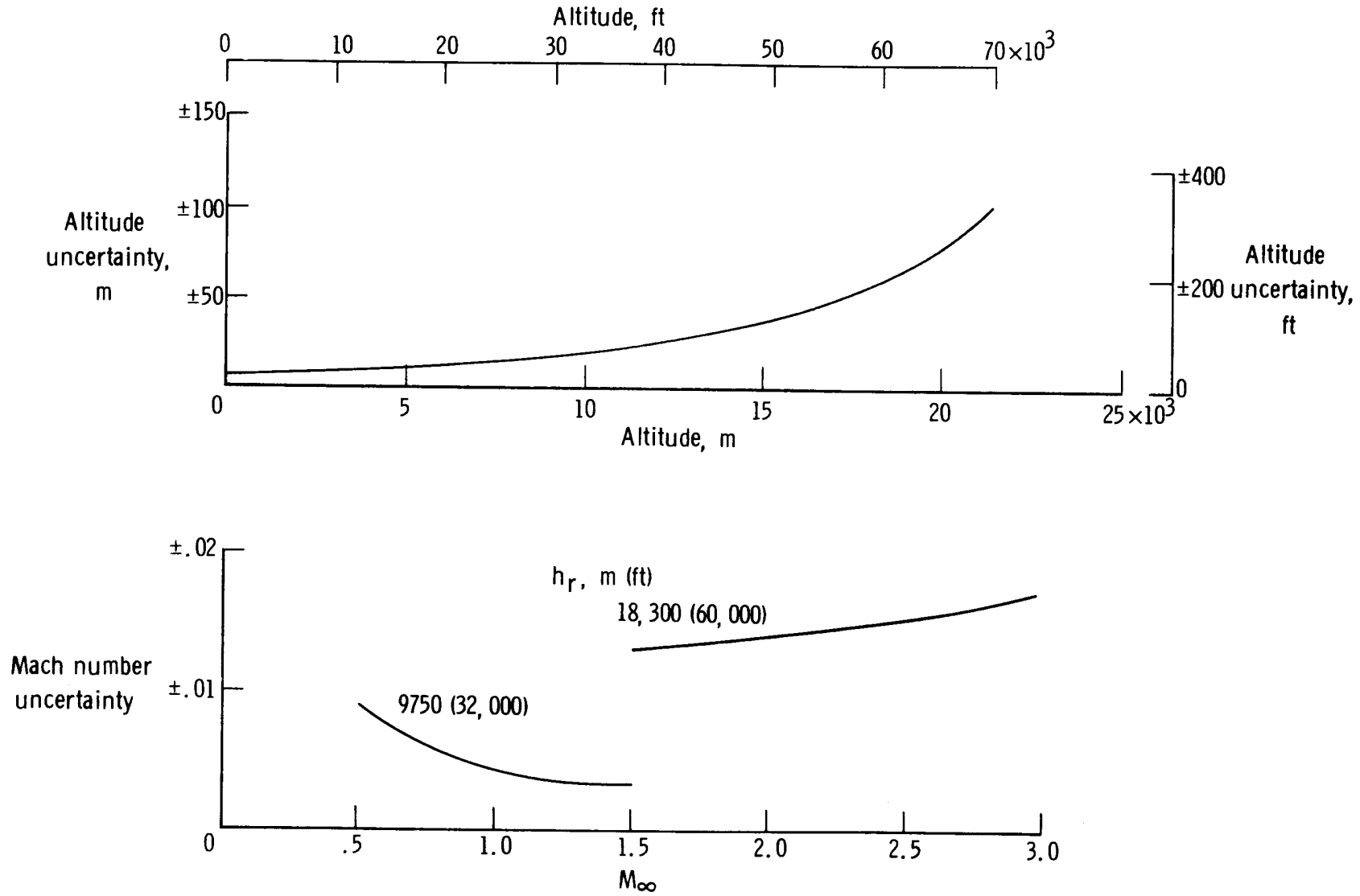

Figure 8. Uncertainties in Mach number and altitude resulting from inaccuracies in the airspeed pressure transducers used on the XB-70 airplane.

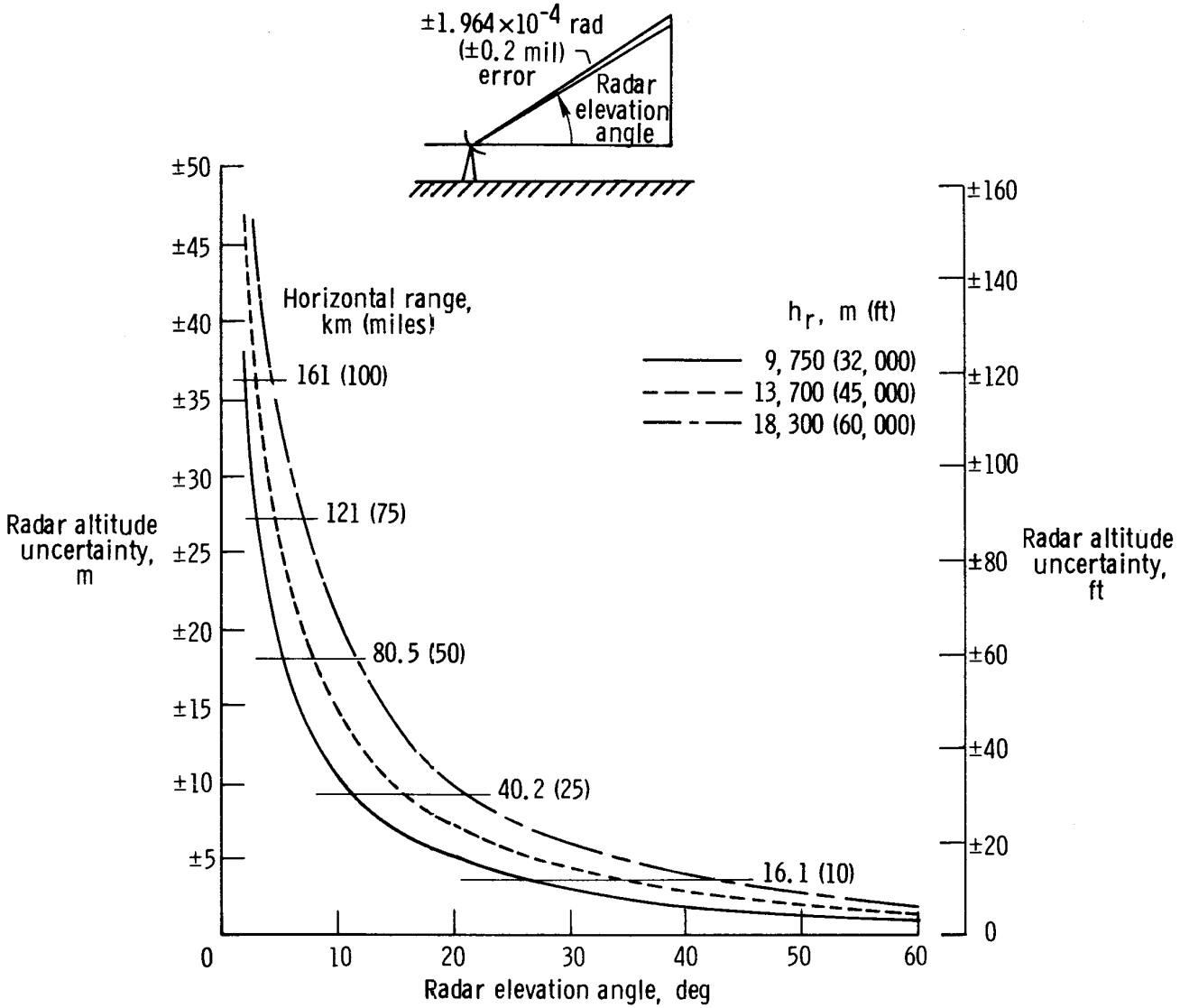

Figure 9. Effect of $\pm 1.964 \times 10^{-4}$-radian (±0.2-mil) error in radar elevation angle on radar altitude uncertainty.

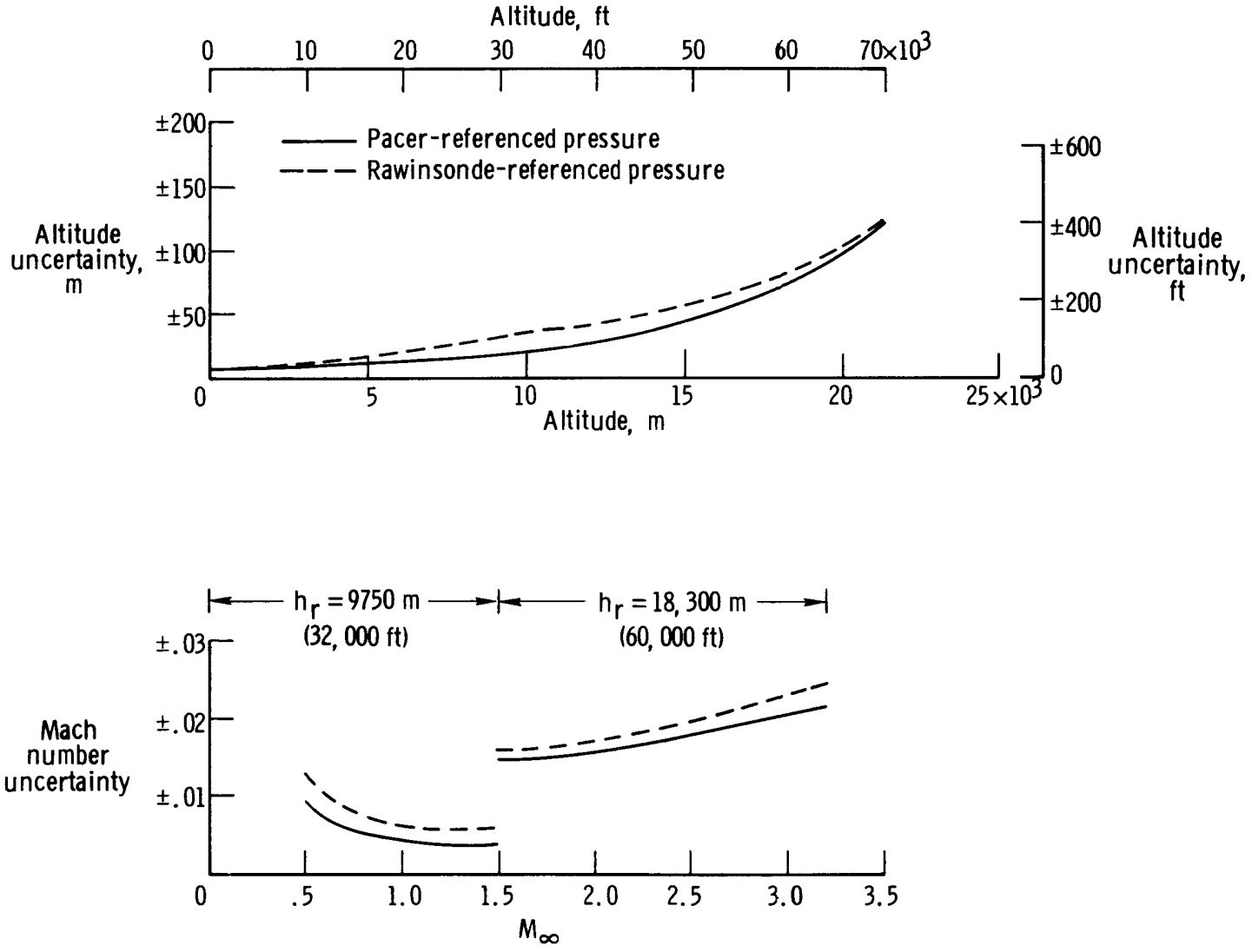

Figure 10. Effect of reference pressure error on the uncertainties in Mach number and altitude measurements.

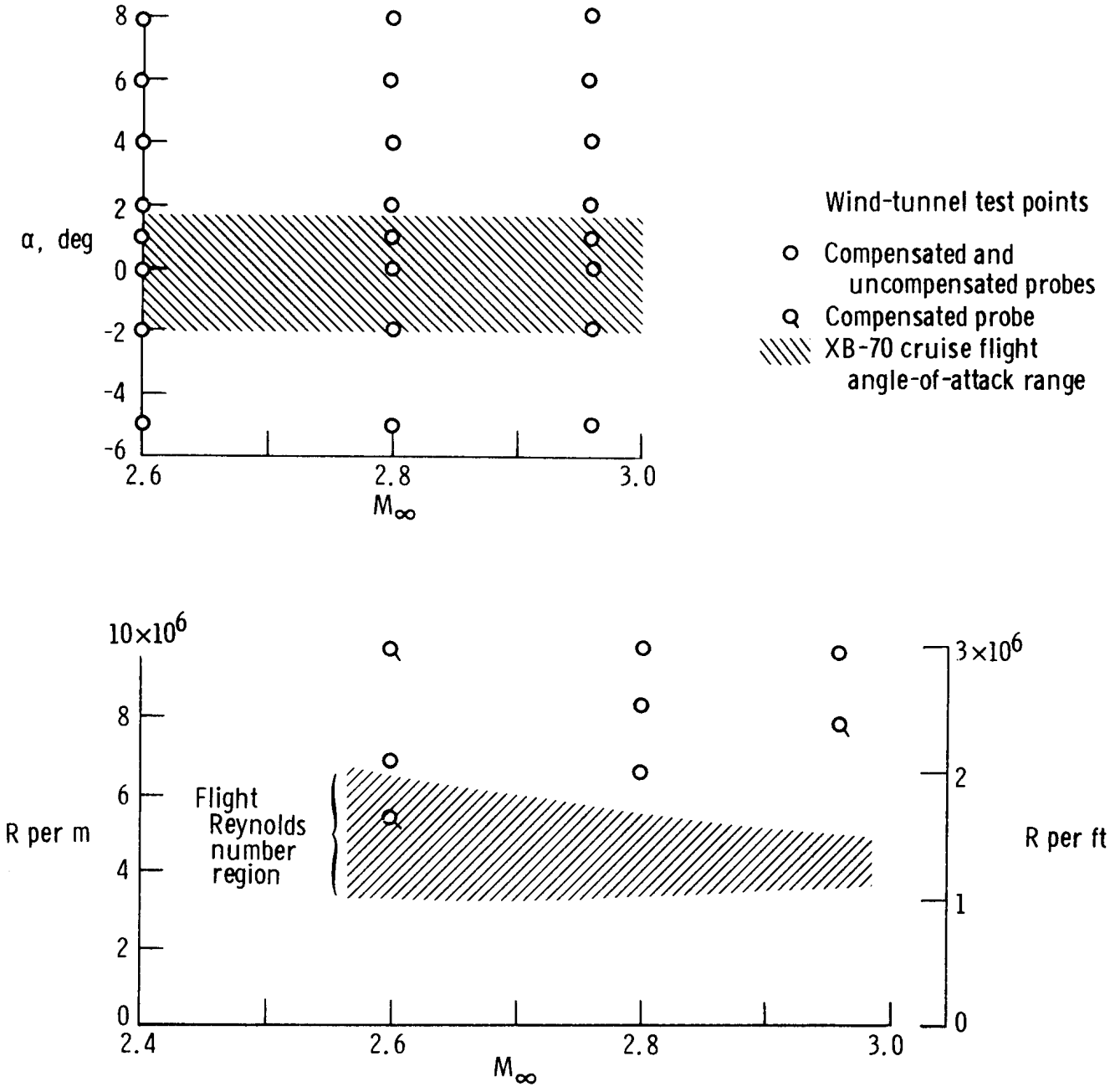

Figure 11. Comparison of wind-tunnel test points with the XB-70 flight-test region.

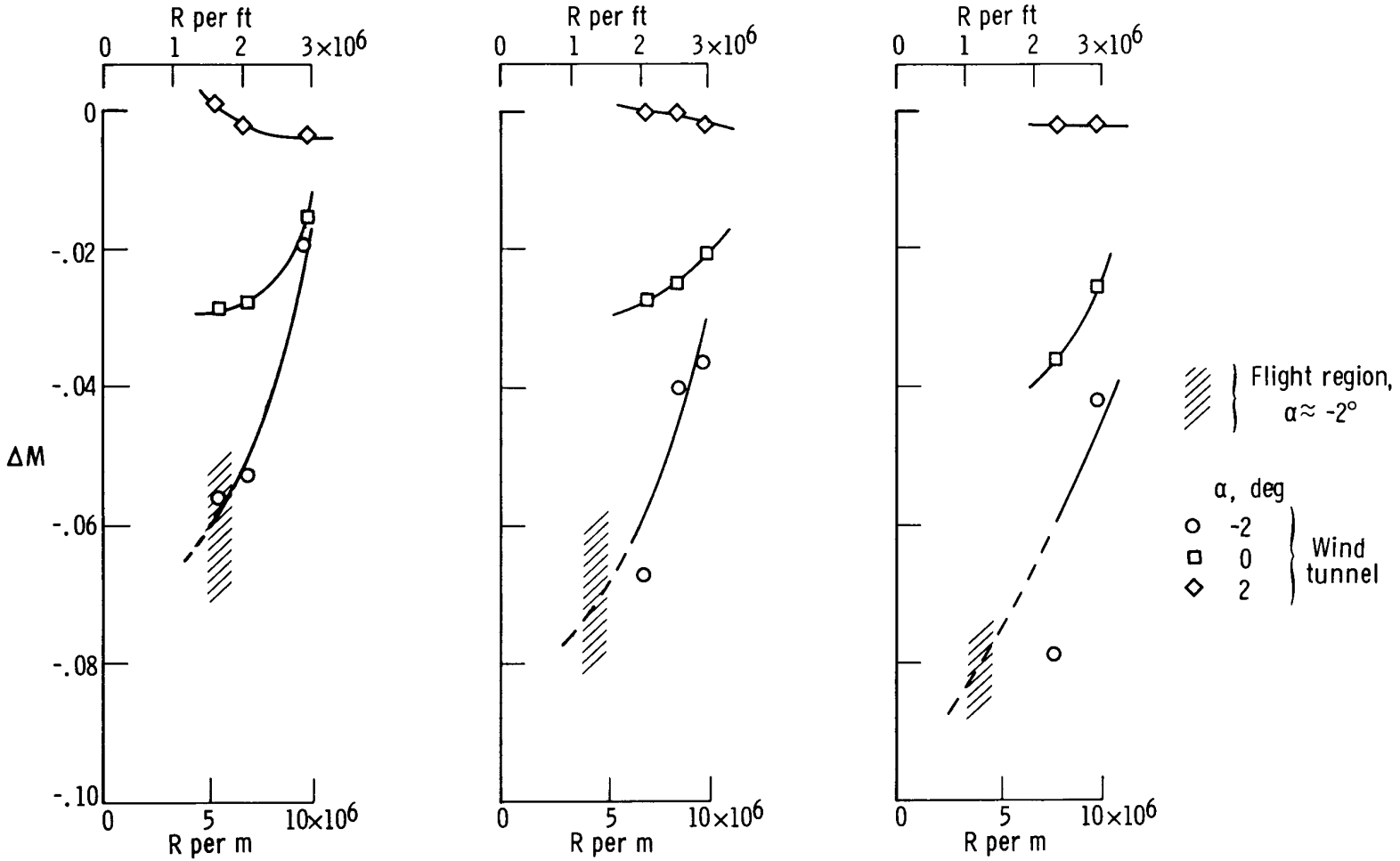

(a) $M_\infty = 2.60$.

(b) $M_\infty = 2.80$.

(c) $M_\infty = 2.96$.

Figure 12. Variation of Mach number position error for the compensated probe with Mach number, Reynolds number, and angle of attack.

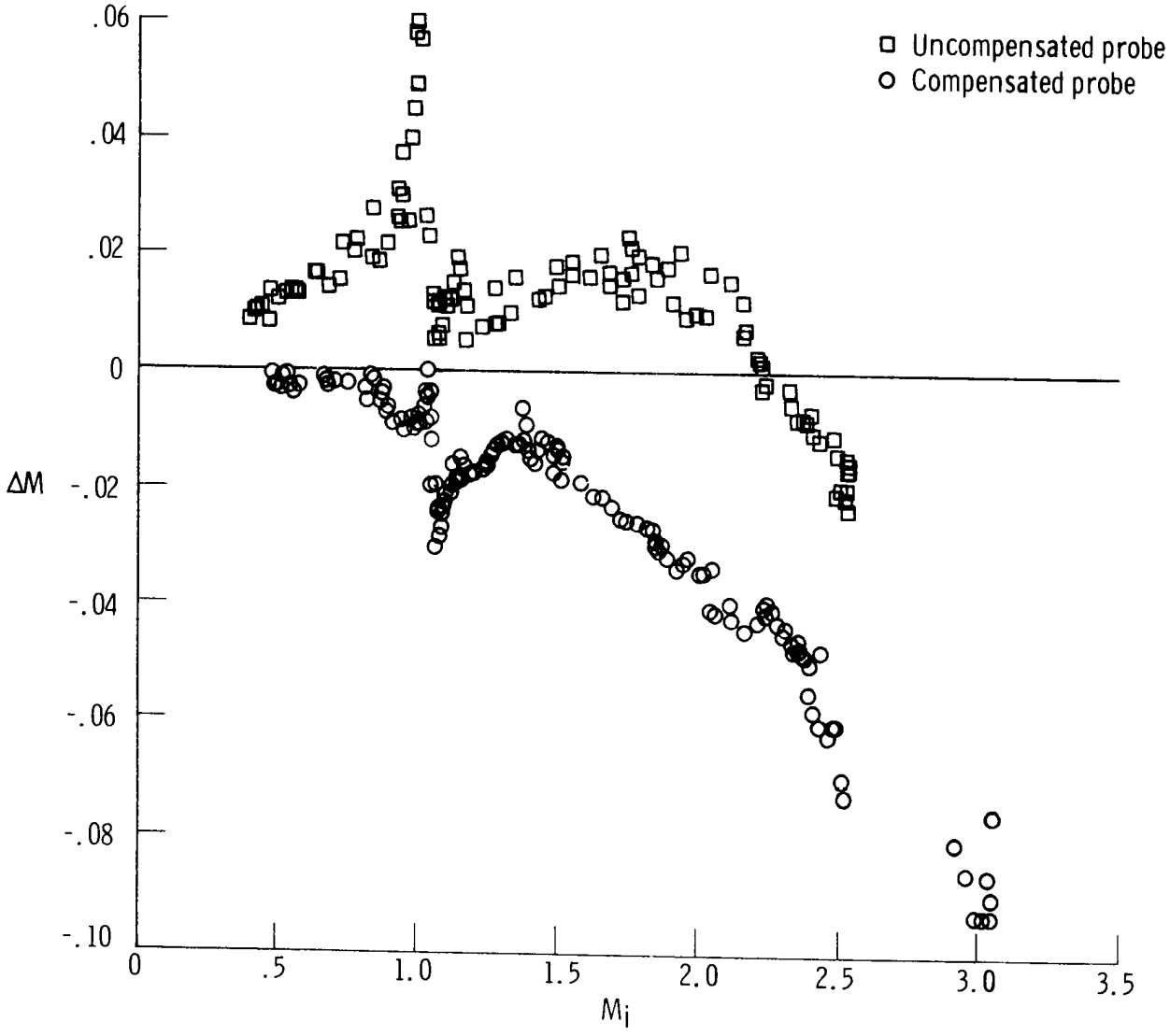

Figure 13. Variation of Mach number position error with Mach number for the two pitot-static probes used on the XB-70. S_1/S_2 configuration.

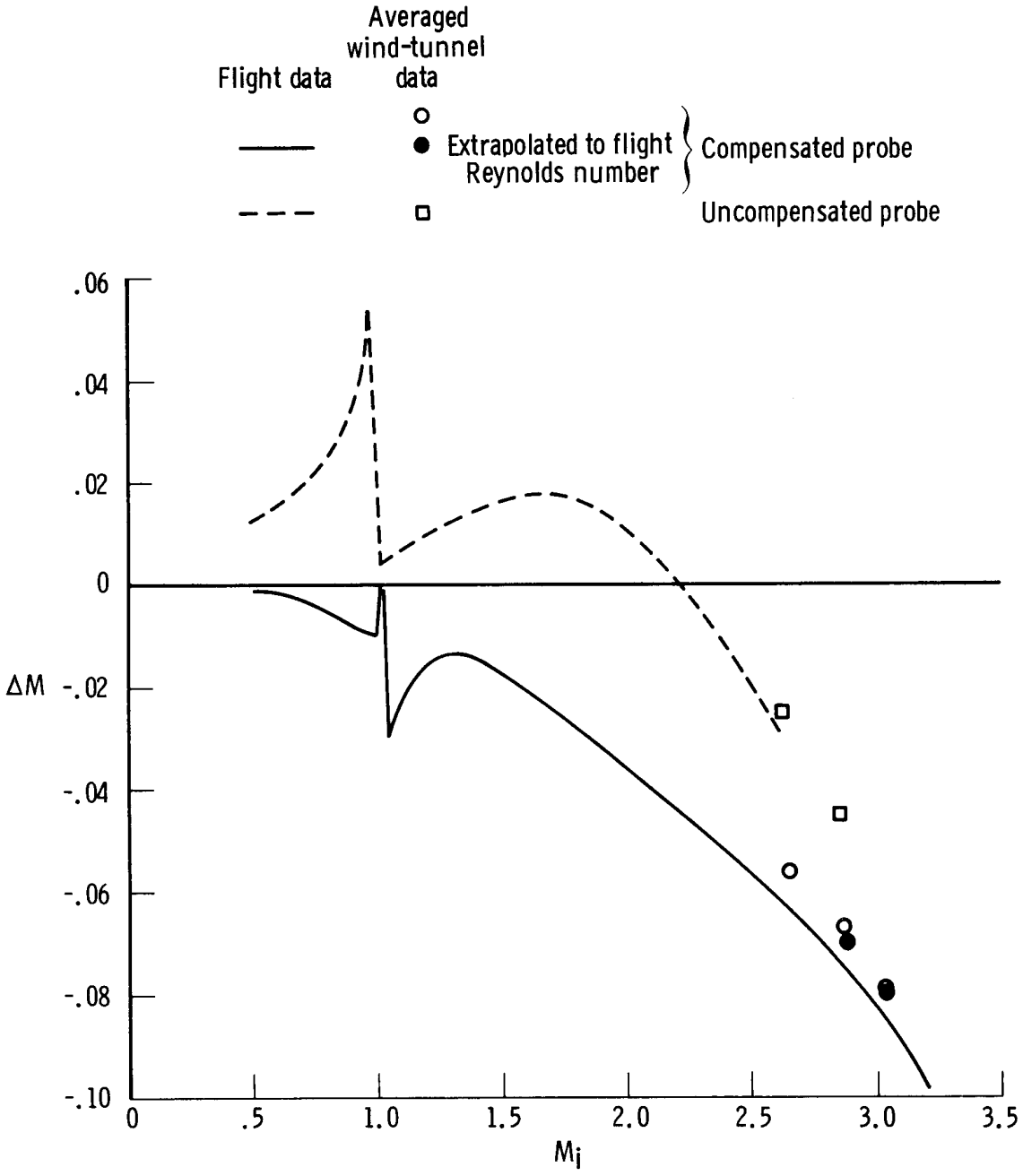

(a) Variation of Mach number position error with indicated Mach number.

Figure 14. Faired position-error calibrations for the XB-70 compensated and uncompensated pitot-static probes. S_1/S_2 configuration.

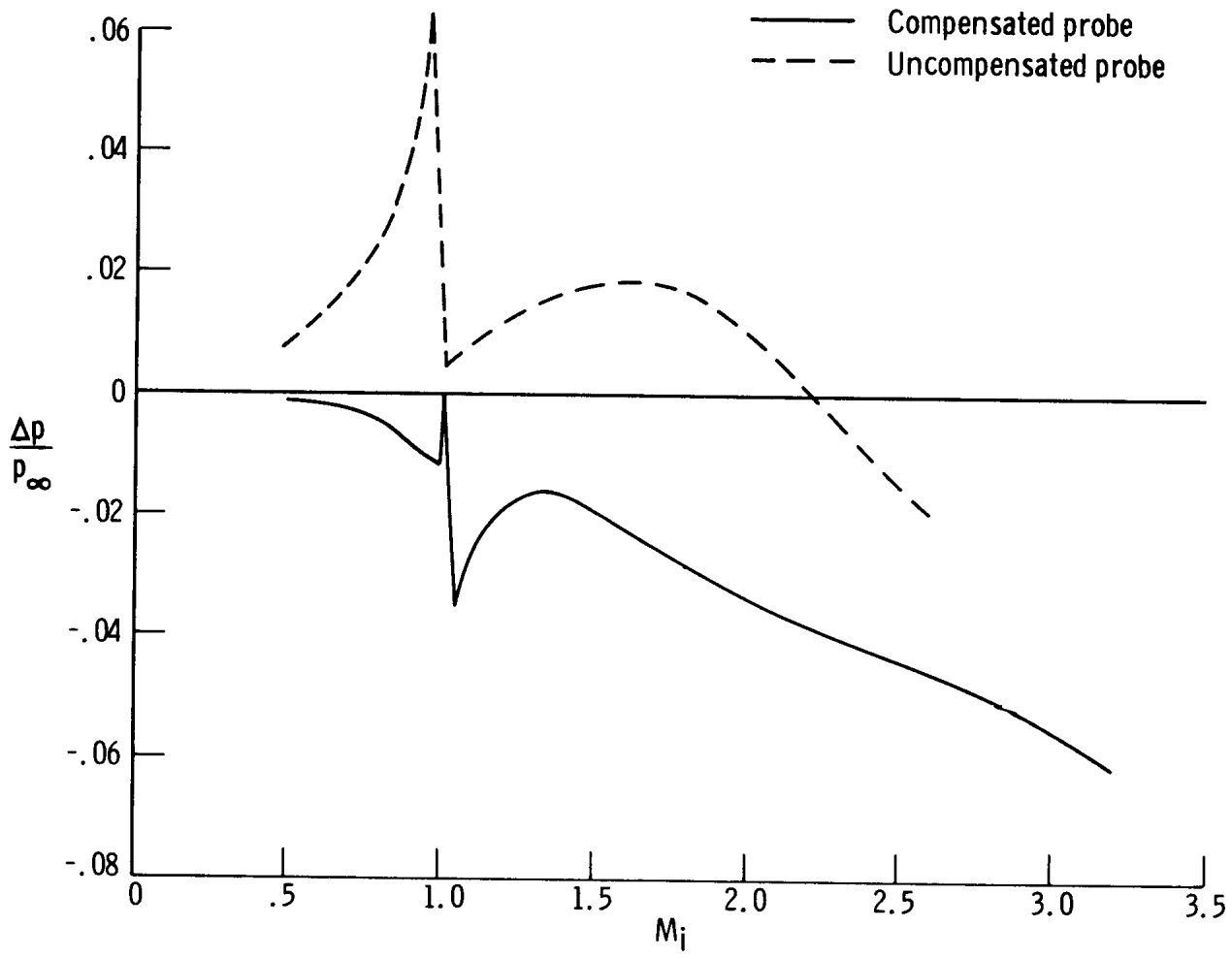

(b) Variation of static-pressure position error with indicated Mach number.

Figure 14. Continued.

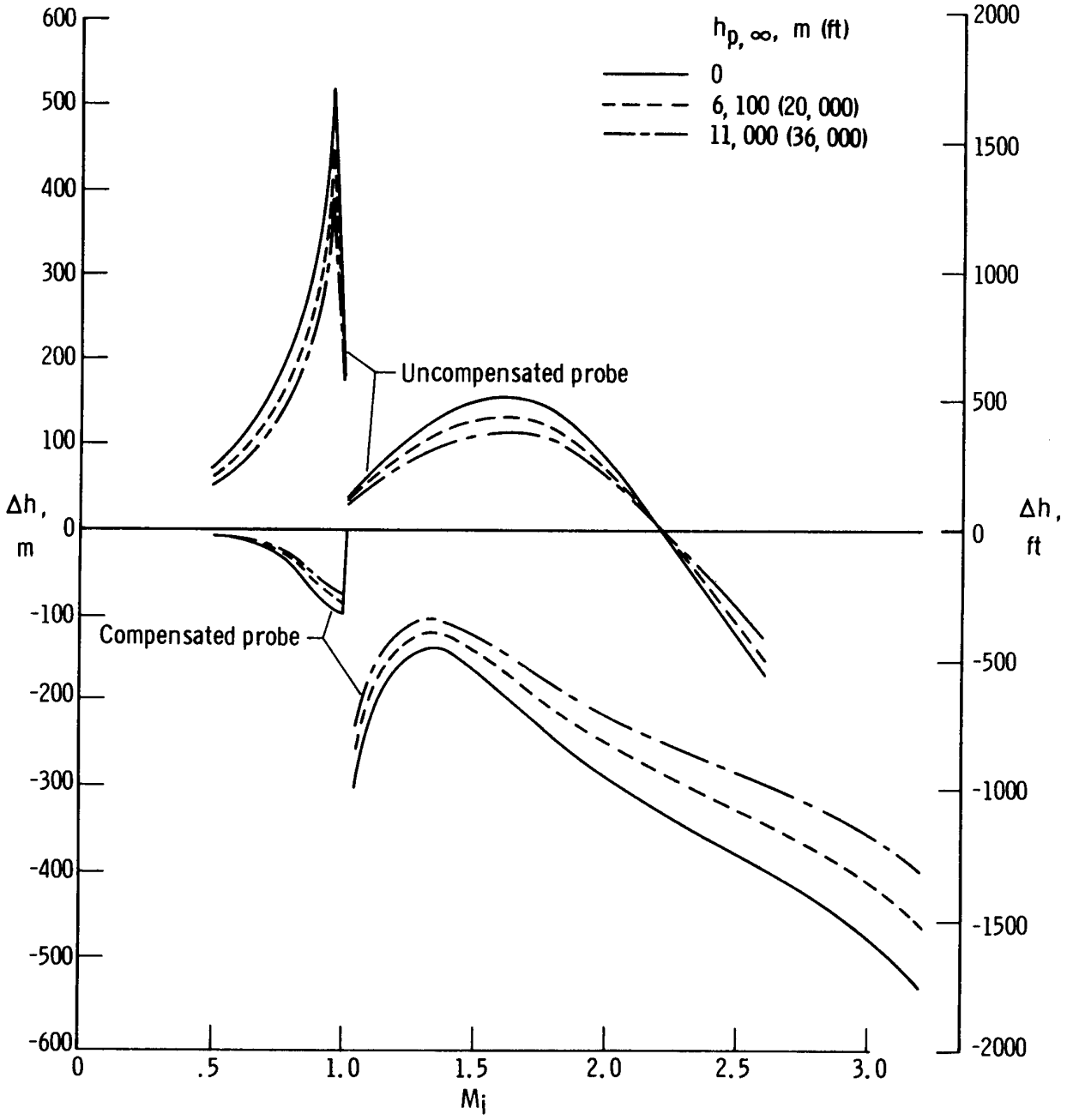

(c) Variation of pressure-altitude position error with indicated Mach number.

Figure 14. Concluded.

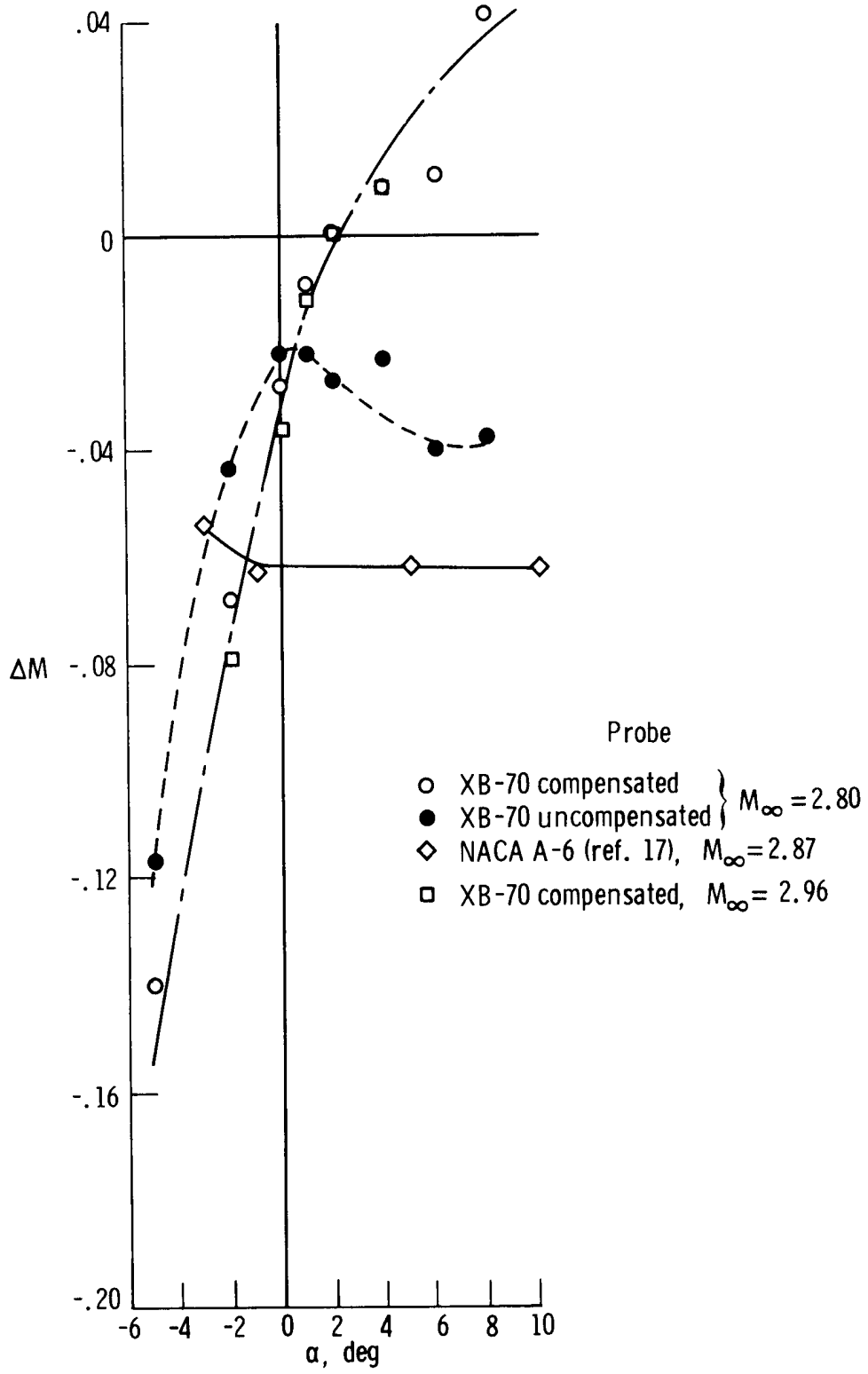

Figure 15. Effect of angle of attack on the Mach number position error for three types of pitot-static airspeed probes as obtained from Langley wind-tunnel calibrations.

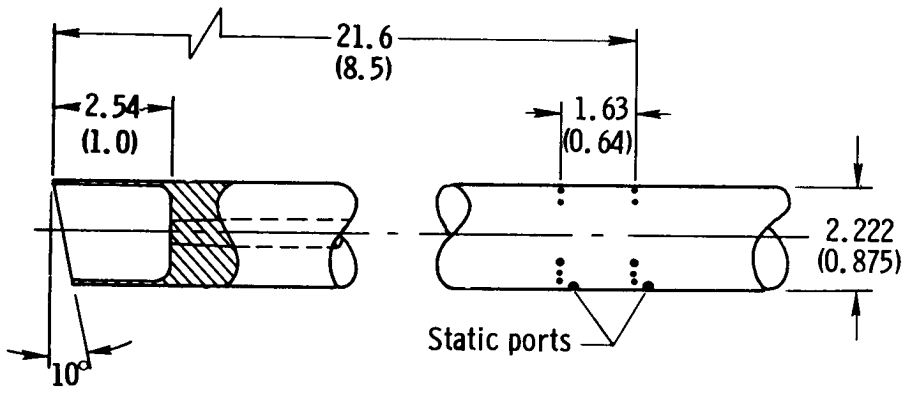

(a) NACA A-6 probe.

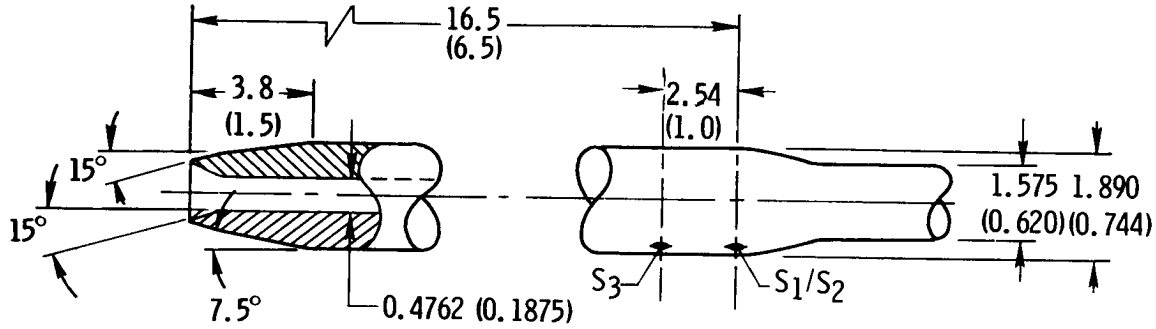

(b) XB-70 compensated probe.

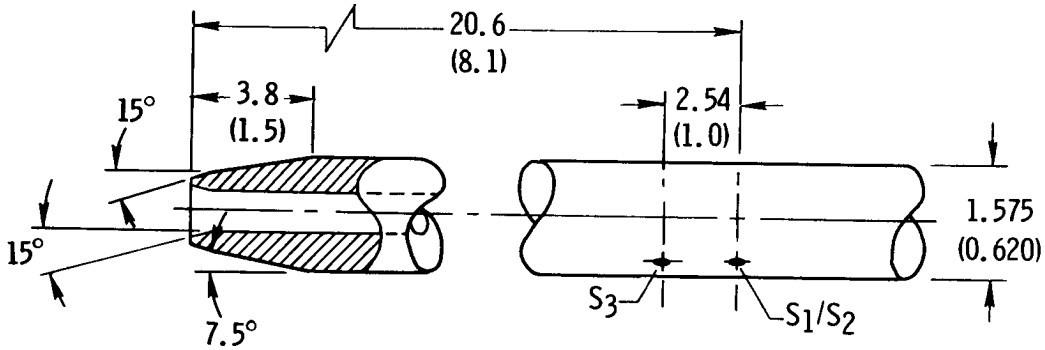

(c) XB-70 uncompensated probe.

Figure 16. Comparison of tips and static-pressure orifice locations for three types of pitot-static probes. Dimensions in centimeters (inches) unless otherwise noted.

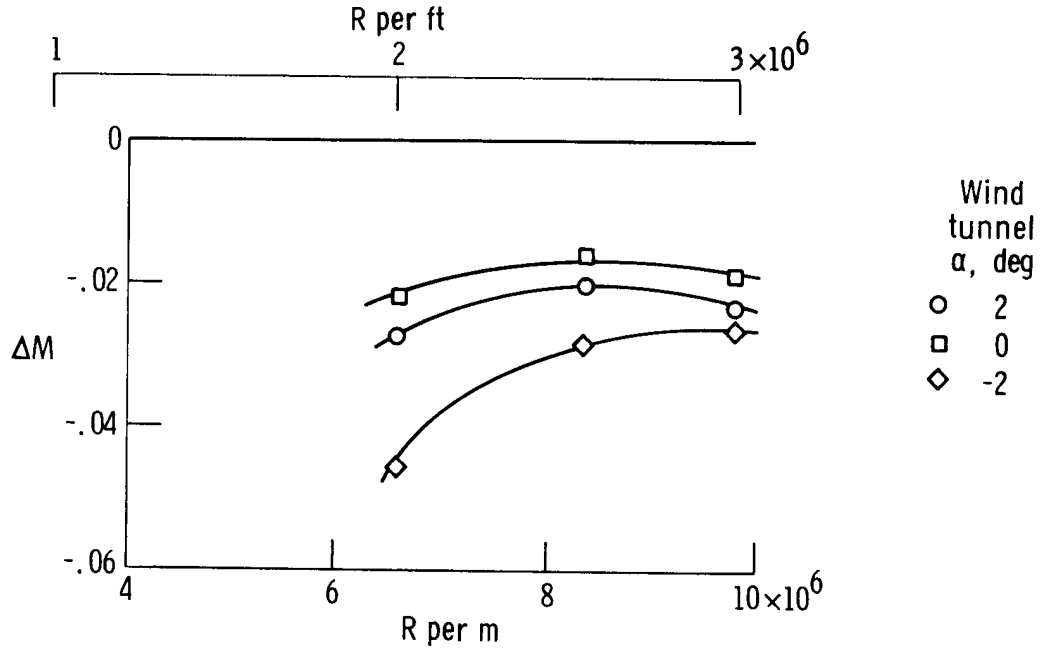

(a) Uncompensated probe.

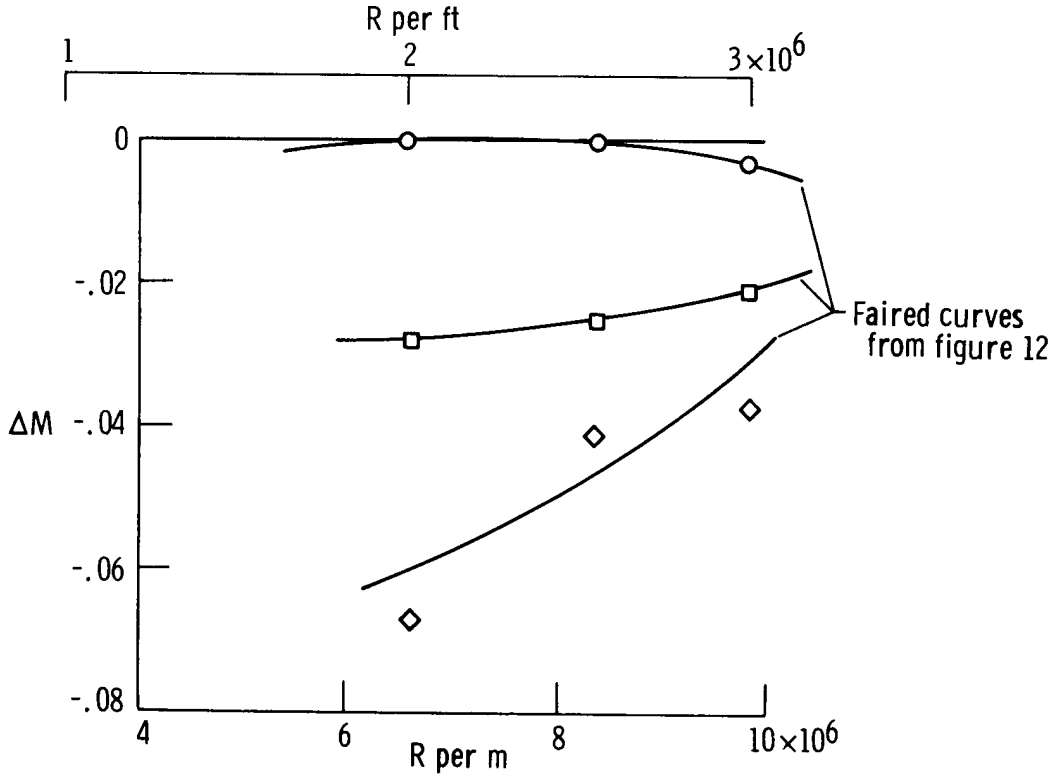

(b) Compensated probe.

Figure 17. Effect of Reynolds number on Mach number position error for the compensated and the uncompensated pitot-static probes as obtained from wind-tunnel data. $M_\infty = 2.8$; S_1/S_2 configuration.

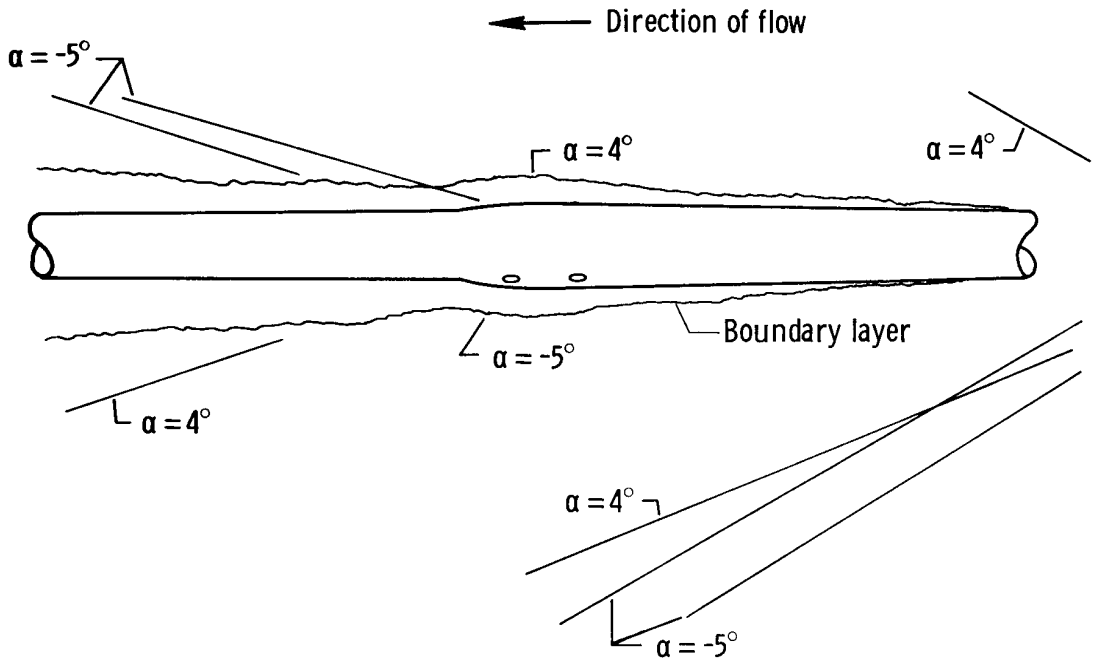

(a) Turbulent boundary layer over static ports. R per meter = 13.1×10^6 (R per foot = 4×10^6).

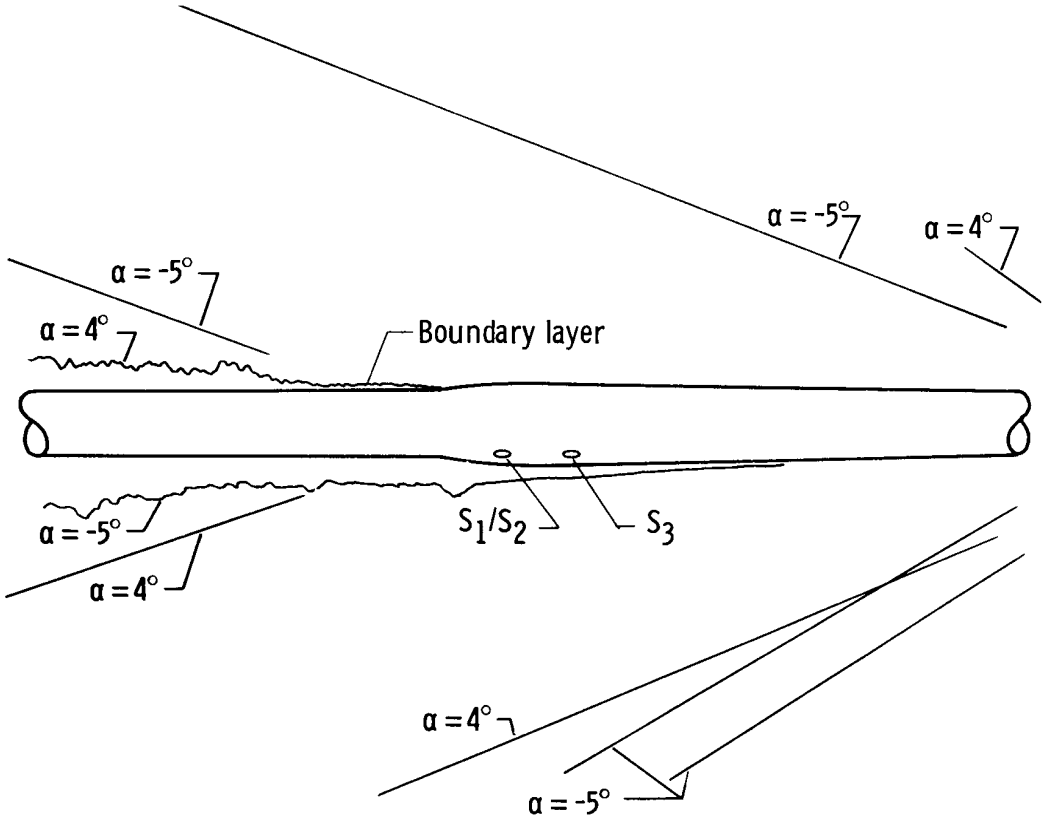

(b) Laminar boundary layer over static ports. R per meter = 4.862×10^6 (R per foot = 1.482×10^6).

Figure 18. Schematic drawing of the shock-wave boundary-layer interaction on the XB-70 compensated pitot-static probe for two Reynolds numbers at a Mach number of 2.6.

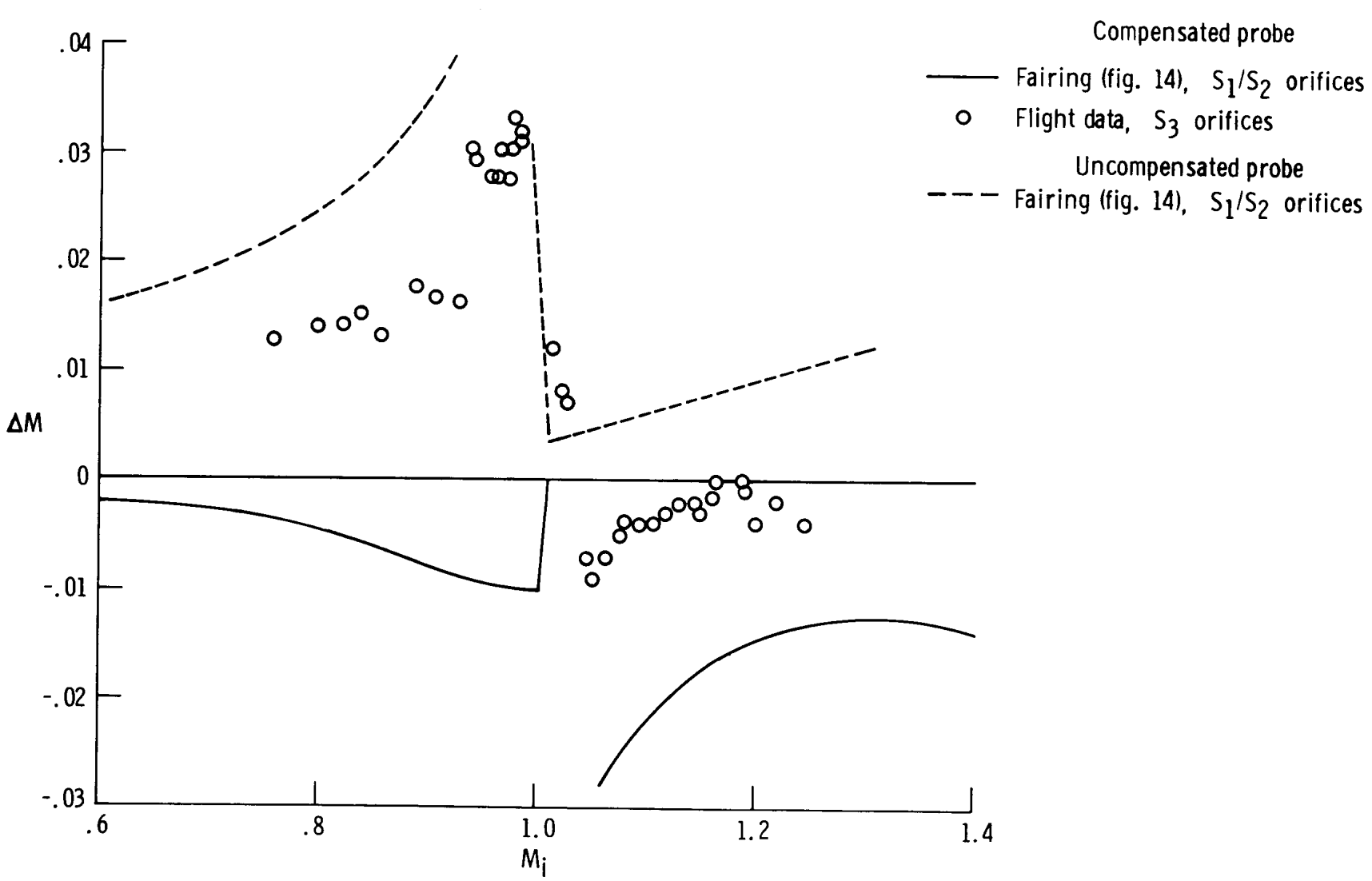

Figure 19. Comparison of position errors for the S_3 orifices on the compensated pitot-static probe with those for the S_1/S_2 orifices on the compensated and uncompensated pitot-static probes.

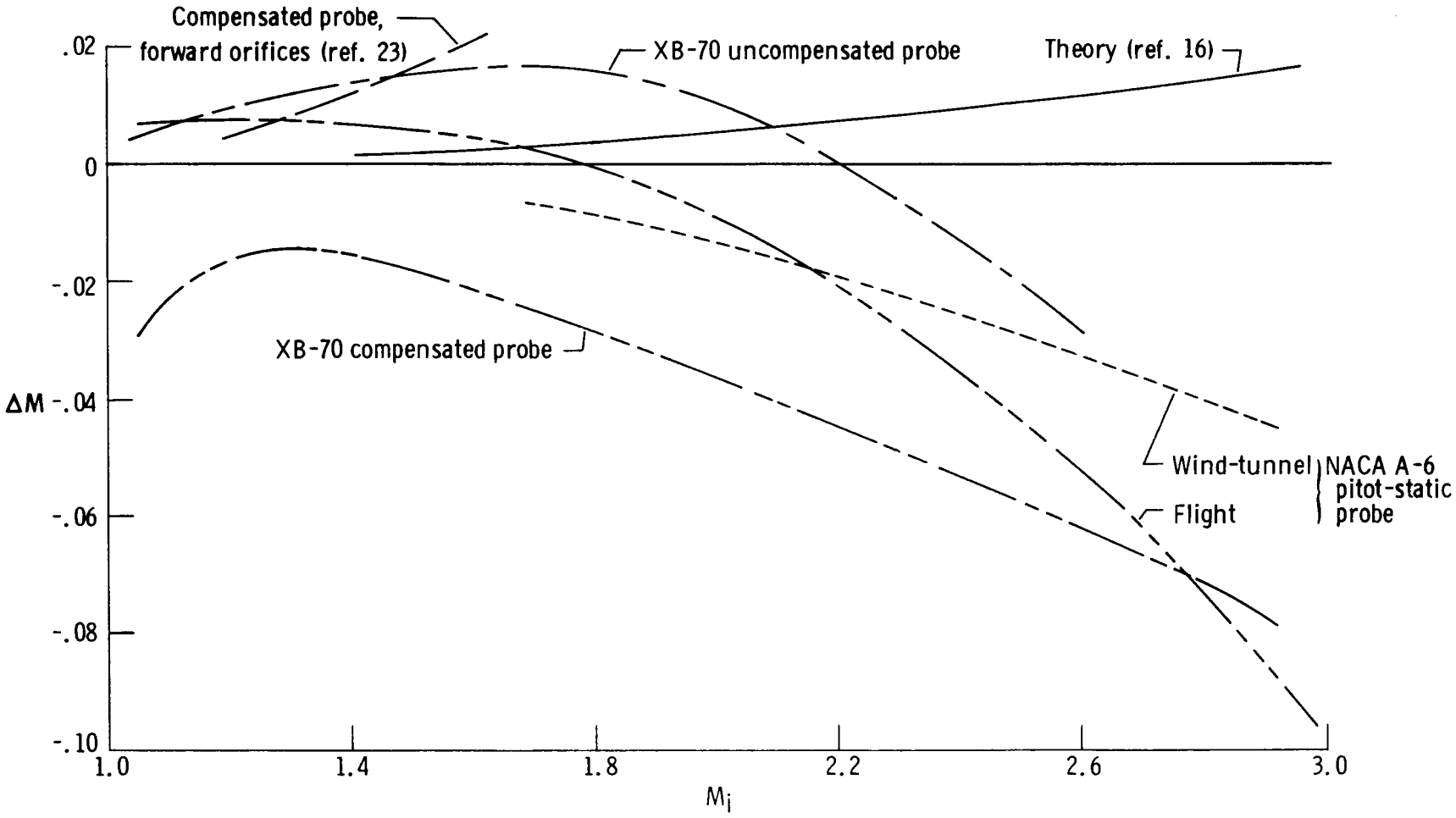

Figure 20. Comparison of supersonic position errors obtained from theory, wind-tunnel tests, and flight data for several types of nose-boom-mounted pitot-static airspeed probes.

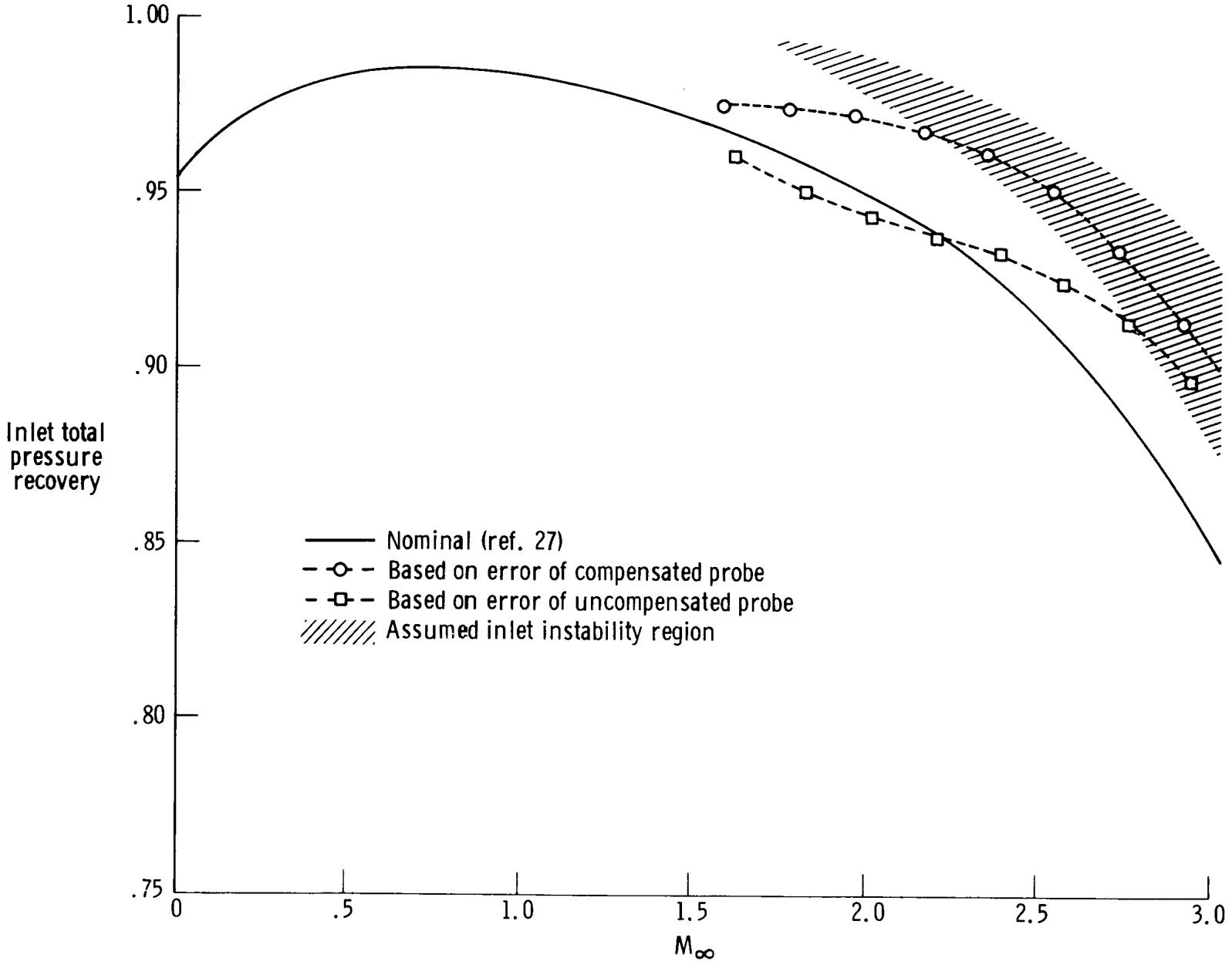

Figure 21. Effects of airspeed probe position error for the S_1/S_2 configuration in establishing supersonic inlet pressure recovery.